A review on thermoelectric renewable energy: Principle parameters that affect their performance

Mohamed Hamid Elsheikh [a,c,*], Dhafer Abdulameer Shnawah [a], Mohd Faizul Mohd Sabri [a], Suhana Binti Mohd Said [b], Masjuki Haji Hassan [a], Mohamed Bashir Ali Bashir [a], Mahazani Mohamad [b]

[a] Department of Mechanical Engineering, University of Malaya, 50603 Kuala Lumpur, Malaysia
[b] Department of Electrical Engineering, University of Malaya, 50603 Kuala Lumpur, Malaysia
[c] Department of Mechanical Engineering, University of Bahri, 13104 Khartoum, Sudan

A R T I C L E   I N F O

A B S T R A C T

Developing thermoelectric materials with superior performance means tailoring interrelated thermo-electric physical parameters – electrical conductivities, Seebeck coefficients, and thermal conductivities – for a crystalline system. High electrical conductivity, low thermal conductivity, and a high Seebeck coefficient are desirable for thermoelectric materials. Therefore, knowledge of the relation between electrical conductivity and thermal conductivity is essential to improve thermoelectric properties. In general, research in recent years has focused on developing thermoelectric structures and materials of high efficiency. The importance of this parameter is universally recognized; it is an established, ubiquitous, routinely used tool for material, device, equipment and process characterization both in the thermoelectric industry and in research. In this paper, basic knowledge of thermoelectric materials and an overview of parameters that affect the figure of merit ZT are provided. The prospects for the optimization of thermoelectric materials and their applications are also discussed.

© 2013 Elsevier Ltd. All rights reserved.

Contents

* Corresponding author at: University of Malaya, Department of Mechanical Engineering, Jalan University, 50603 Kuala Lumpur, Malaysia. Tel.: +60 122 567 021; fax: +60 379 675 317.
E-mail address: mohdelsheikh84@gmail.com (M. Hamid Elsheikh).

1. Introduction

The search for cleaner, more sustainable energy sources is an ever-growing global concern because of escalating energy costs and global warming associated with fossil fuel sources [1–5]. Among the viable technologies for this purpose, thermoelectric (TE) energy converters are of increasing interest because these solid-state devices can transform heat given off from sources such as power plants, factories, motor vehicles, computers or even human bodies into electric power using the Seebeck effect [6–12]. The many advantages of this energy-conversion phenomenon include solid-state operation, the absence of toxic residuals, vast scalability, maintenance-free operation vis-à-vis the lack of moving parts or chemical reactions, and a long life span of reliable operation [13–16]. Conversely, solid-state thermoelectric devices can also change electrical energy into thermal energy for cooling or heating using the Peltier effect. Compared to traditional refrigeration and heating mechanisms, solid-state thermoelectric energy converters have the advantage of simplicity; they produce no vibrations and are highly scalable. Furthermore, because TE devices use no refrigerants or working fluids, they may be expected to produce negligible direct emissions of greenhouse gases over their lifetimes [17]. However, because of their low efficiency, current TE materials have found limited commercial application. A brief perusal of the possibilities is illustrated in Fig. 1, where the different scales of energy generation that are represented are relevant to different applications [18]. The problem remains that the efficiency of today's thermoelectric material is inadequate to compete with conventional power generation and refrigeration [19]. Moreover, the growing need for alternative power sources is driving a growing interest in developing a new

generation of thermoelectric materials. To become competitive with present, novel thermoelectric materials will need to increase in efficiency by a factor of three over the present values [20]. Therefore, this review discusses basic knowledge of thermoelectric materials, their applications and an overview of the parameters that affect their performance.

2. Thermoelectric properties

Thermoelectric devices can convert thermal energy from a temperature gradient into electrical energy. This phenomenon was discovered in 1821 and is called the "Seebeck effect," while the reverse counterpart of this phenomenon was discovered by Peltier in 1834 [13]. As knowledge of thermoelectrics increased, the most important discoveries were related to material properties. In 1911, Altenkirch derived the thermoelectric efficiency, now known simply as Z, or the thermoelectric figure of merit. The thermoelectric efficiency can be non-dimensionalized by multiplying by the absolute temperature T, which yields the most common form of thermoelectric efficiency, ZT, also known as the dimensionless figure of merit. This value is given as

$$ZT = \alpha^2 \sigma T / K \tag{1}$$

where α is the Seebeck coefficient, σ is the electrical conductivity, and K is the thermal conductivity. These three transport parameters α, σ and K depend upon one another as a function of the band structure, carrier concentration and many other factors that are discussed later in this paper; Fig. 2 illustrates the three main parameters, including the carrier concentration [21]. In particular, α and σ generally vary in a reciprocal manner, making any improvement in the figure of merit Z difficult [22]. In addition,
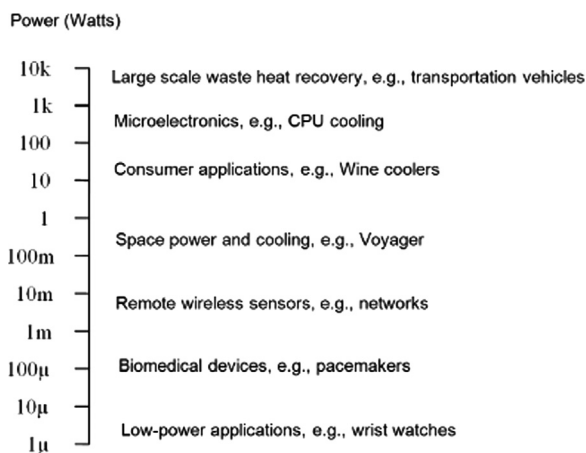
Fig. 1. Thermoelectric materials can be put to use in various energy conversion applications, encompassing ten orders of magnitude in power, as illustrated in the text [18].
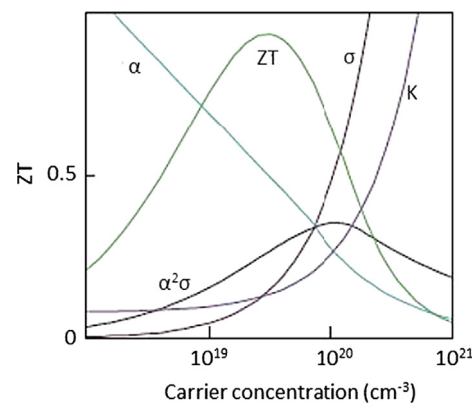
Fig. 2. Maximizing the efficiency (ZT) of a thermoelectric involves a compromise of thermal conductivity (k; plotted on the y-axis from 0 to a top value of 10 W m^{-1} K^{-1}) and Seebeck coefficient (S or α; 0–500 μV K^{-1}) with electrical conductivity (σ; 0–5000 Ω^{-1} cm^{-1}) [21].

the electrical conductivity and the Seebeck coefficient are inversely related, so it is not generally possible to increase the thermoelectric power factor above a particular optimal value for a bulk material [23]. However, ideal thermoelectric materials would have a high electrical conductivity to allow the conduction of electricity, which would create a potential difference across the sample, and a low thermal conductivity to maintain the temperature gradient between the hot and cold side [24]. Early work in thermoelectrics resulted in very small values of Z because the materials being used (mostly metals) did not possess ideal thermoelectric properties; i.e., metals possess both high electrical conductivity and high thermal conductivity. Most traditional materials exhibit a correlation between electrical and thermal conductivity. A material that conducts electricity well, such as a metal, also conducts heat well, and a material that insulates heat, such as glass or ceramic, also insulates electricity [21].

Many years of effort to increase ZT have not yet led to a fundamental breakthrough. In fact, the history of thermoelectric materials can be characterized by the progress in increasing ZT, as shown in Fig. 3 [25]. Thus, for devices operating at room temperature ($T \approx 300$ K), traditional thermoelectric materials, such as bismuth telluride (Bi_2Te_3) and lead telluride (PbTe), possess values of $ZT \approx 1$ [26]. In recent years, work by Venkatasubramanian et al. [27] and Harman et al. [28] using superlattices and quantum dots based on these materials has increased their room room-temperature ZT to ~ 2–2.4. These improvements in performance are primarily the result of a reduction in lattice thermal

conductivity, and the thermoelectric power factor ($\alpha^2\sigma$) is largely unchanged. For practical purposes, a suitable high-performance TE material should have a ZT of > 4, and the achievement of this goal has remained a formidable challenge [19]. However, commercial materials are available with $ZT \approx 1$.

2.1. The Seebeck coefficient

A temperature difference between two points in a conductor or semiconductor results in a voltage difference between these two points. Stated differently, a temperature gradient in a conductor or semiconductor gives rise to a built-in electric field. This phenomenon is called the Seebeck effect or the thermoelectric effect [29]. The Seebeck coefficient gauges the magnitude of this effect. The thermoelectric voltage developed per unit temperature difference in a conductor is called the Seebeck coefficient or thermopower. Only the net Seebeck voltage difference between different metals can be measured [25]. In fact, it is via the Seebeck effect that thermoelectric devices can act as electrical power generators [30]. A schematic diagram of a simple solid-state thermoelectric refrigerator or power generator operating based on the Seebeck effect is shown in Fig. 4.

The Seebeck coefficient is expressed in units of V/K (or, more commonly, μV/K or μV/°C). It has been found that only a combination of two different materials, a so-called thermocouple, exhibits the Seebeck effect. For two leads of the same material, no Seebeck effect manifests, although both leads intrinsically possess a Seebeck coefficient, for reasons of symmetry. It is, however, present because the Seebeck effect is a bulk property and does not depend on either the specific arrangement of the leads or the material or the specific method of joining them [31]. Metals have different thermoelectric sensitivities, or Seebeck coefficients. For example, iron has a Seebeck coefficient of 19 μV/°C at 0 °C, which means that for every 1 °C difference in temperature, a positive thermoelectric emf (or Seebeck voltage) of 19 μV is induced in iron at temperatures near 0 °C. A negative thermoelectric electromotive force (emf) can also be induced in a metal, so Seebeck coefficients can also have negative values. For example, constantan (a copper–nickel alloy) has a Seebeck coefficient of -35 μV/°C at 0 °C. Generally, most metals possess Seebeck coefficients of 10 μV/K or less, but semiconductor materials are promising for the construction of thermocouples because they have Seebeck coefficients in excess of 100 μV/K. It should be noted that the relation between
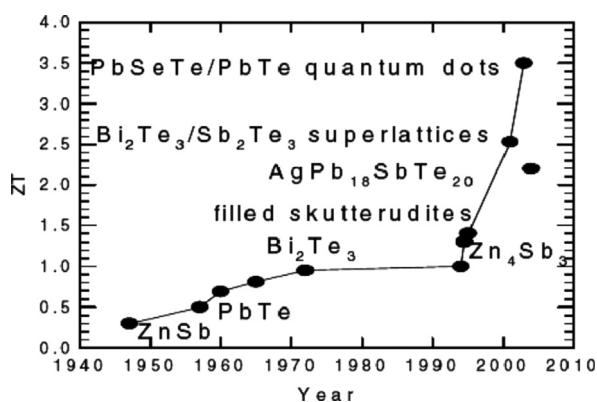
Fig. 3. ZT of many typical thermoelectric materials as a function of year [25].
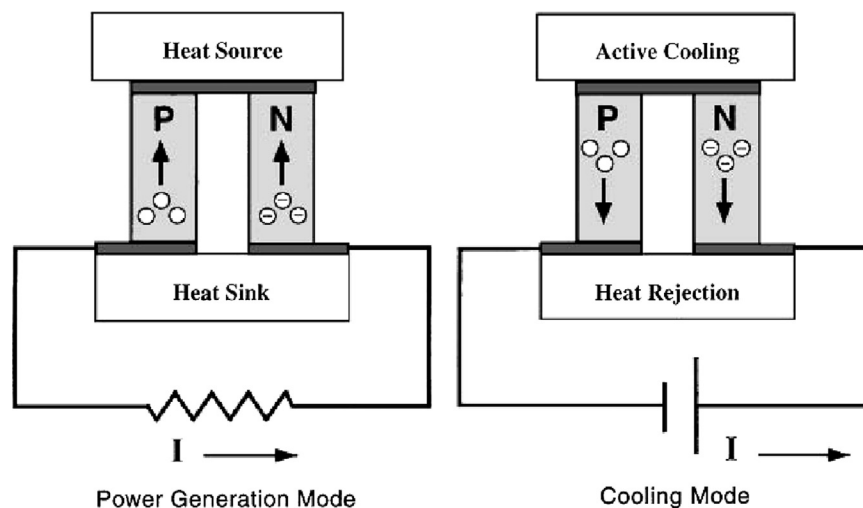

Fig. 4. A thermoelectric modules illustrating the versatility of these materials for use in solid-state thermoelectric refrigeration or in power generation. The thermoelectric module is composed of an n-type and a p-type semiconducting material connected electrically in series through metallic electrical contact pads and thermally in parallel between ceramic ends [30].

the Seebeck voltage and the temperature is linear only for small changes in temperature [30]. For larger temperature ranges, the relationship becomes non-linear. It is therefore important to state the temperature at which the Seebeck coefficient is being specified. However, thermopower ≥ 225 is required to achieve $ZT > 2$ [32].

2.2. Thermal conductivity

A high-quality thermoelectric material must have a high electrical conductivity, a high thermopower, and a low thermal conductivity. Because the first two are determined only by the electronic properties of the material, they are often combined into the quantity $PF = \alpha^2 \sigma$, referred to as the 'power factor.' In contrast, the thermal conductivity $K = K_e + K_L$ in thermoelectrics is the sum of two contributions: (1) electrons and holes transporting heat (K_e) and (2) phonons traveling through the lattice (K_L) [33]. It then follows that the thermoelectric figure of merit can be maximized by maximizing the electrical conductivity and minimizing the thermal conductivity. However, there is a relation between the two: the Wiedemann–Franz law for electrons that obey degenerate and non-degenerate statistics (K_B is the Boltzmann constant, and e is the electron charge):

$$K_e / \sigma = L_0 T \tag{2}$$

$$L_0 = (\pi^2/3)\,(K_B/e)^2 = 2.44 \times 10^{-8} (K^2/V^2) \tag{3}$$

and

$$L_0 = 2(K_B/e)^2 = 1.48 \times 10^{-8} (K^2/V^2) \tag{4}$$

Increasing the electrical conductivity not only produces an increase in the electronic thermal conductivity but also usually decreases the thermopower; optimizing ZT thus turns out to be a challenge. While the power factor can in some cases be increased by varying the concentration of charge carriers in the material, decreasing K and K_L is much more problematic, especially for K_L, which is determined by the structure, rigidity, atomic masses, and other characteristics of the lattice [34]. Because the ZT values of the presently available materials are too low for cost-effective applications, various efforts have been made to improve them. The idea of reducing the K_L of a compound by substituting the crystal lattice with an amorphous (glass-like) structure has been suggested, and the phonon-glass electron-crystal (PGEC) concept, which was first introduced by Slack and discussed in detail in a review by Nolas et al. [30] and has become a general guideline for the development new thermoelectric materials, is at the heart of the investigation into the skutterudite material system for thermoelectric applications. A PGEC material would possess electronic properties similar to those normally associated with a good semiconductor single crystal but would have thermal properties akin to those of an amorphous material.

It is believed that the ideal thermoelectric material would have regions of its structure composed of a high-mobility semiconductor, which provides the electron-crystal electronic structure, interwoven with a phonon glass. The phonon-glass region would be ideal for hosting dopants and disordered structures without disrupting the carrier mobility in the electron-crystal region [35]. The thermal conductivity of a semiconductor material is related to its position in the periodic table, i.e., for a larger mean atomic weight, the thermal conductivity is lower. This behavior has been attributed to the increase in density causing the velocity of sound in the crystal to decrease, leading to a subsequent decrease in thermal conductivity [36]. The most widely used commercial thermoelectric material is bulk Bi_2Te_3 and its alloys with Sb, Se, and so on, which exhibit $ZT \approx 1$. It is difficult to scale bulk Bi_2Te_3 to large-scale energy conversion, but fabricating synthetic nanostructures for this purpose is even more

difficult and expensive. Conversely, the most common semiconductor, Si, is abundant and widely used in the electronics industry, and a large industrial infrastructure exists for the low-cost and high-yield processing of Si. Bulk Si, however, has a high k (~ 150 W m^{-1} K^{-1} at room temperature), yielding $ZT \approx 0.01$ at 300 K [37]. Increasing ZT via the reduction of K, by reducing the lattice contribution to the thermal conductivity, is a powerful concept. The most important factors that can aid in accomplishing this are (i) the use of compounds with complex crystal structures, (ii) the presence of heavy atoms weakly bonded to the structures, (iii) the existence of inclusions and/or impurities, (iv) the formation of solid solutions and (v) the existence of a large number of grain boundaries [38]. The introduction of nanostructure has also become a potential tool for reducing K and consequently increasing ZT. This concept has revolutionized the field of TE because, the utilization of nanostructures has led to the achievement of ZT values of approximately 1–2 compared to <1 for bulk materials. The nanostructured $Bi_xSb_{2-x}Te_3$ have been shown to exhibit significantly improved $ZT \approx 1.4$ at 100 °C, mostly because of the reduced K_L [37]. However, it is difficult to scale up these superlattices for large-volume energy-conversion applications because of limitations in both heat transfer and cost. Joshi et al. [39] investigated the enhanced thermoelectric figure of merit in nanostructured p-type silicon germanium bulk alloys and found that this ZT enhancement is most likely attributable to the increased phonon scattering at the grain boundaries and crystal defects formed by lattice distortion, with some contribution from the increased electron power factor at high temperatures.

2.3. Electrical resistivity (ρ)

Electrical resistivity is an important material-dependent property that is usually a function of temperature. The value of ρ at room temperature is indicative of whether a material is an insulator (ρ is on the order of $10^6 \, \Omega$ m or more) or a metal (ρ is on the order of $10^{-6} \, \Omega$ m or less). In the latter case, if the lattice was perfect, the electron would travel infinitely through it, and the material would only exhibit finite conductivity because of the thermal motion of the lattice and the effect of impurities [36]. The resistivity of a semiconductor material falls between the metal and insulator regimes. It has been found that the optimum range of electrical resistivity for a thermoelectric material is from 10^{-3} to $10^{-2} \, \Omega$ m [40]. Variations in the electrical resistivity of a semiconductor depend on changes in the carrier concentration and the mean free path of the charge carriers. The charge carriers are reflected/scattered by the surface of the material when they reach it [41]. To achieve low electrical resistivity in semiconductors, the lattice should have nearly infinite conductance at low temperatures, but in reality, the conductivity of semiconductors is very low at low temperatures because of the limited number of free electrons [36]. Moreover, the analysis of the temperature dependence of the electrical resistivity in intermetallic compounds is a powerful tool for obtaining information regarding the intrinsic properties of these materials. Depending on the temperature range considered, one can draw certain conclusions regarding the scattering of electrons on the thermal excitations of the lattice [42].

3. Categories of TE material

Thermoelectric materials comprise a huge family, including various materials from semimetals and semiconductors to ceramics, containing various crystalline forms from monocrystals and polycrystals to nanocomposites and covering varying dimensions from bulk, films and wires to clusters. Recently, certain polymers have also been shown to exhibit interesting thermoelectric material properties.

3.1. Metal-based thermoelectrics

The history of applications of thermoelectric materials is strongly associated with their efficiency. The earliest application of the thermoelectric effect was in metal thermocouples, which have been used to measure temperature and radiant energy for many years [25]. However, metals possess very high electrical conductivity and very high thermal conductivity. Several TE materials containing heavy metals such as Bi, Sb, Pb and Te have been developed so far; these materials are mostly toxic and unstable at high temperatures ($\sim$1000 K) [43]. Therefore, metal oxides that exhibit good TE performance are in high demand because metal oxides are environmentally friendly and essentially stable at high temperatures [43]. Watanabe et al. [44] measured the temperature dependence of the electrical resistivity and the thermoelectric power of $(Ni_{1-x}M_x)Mn_2O_4$ (M=Zn and Mg, $x=0$, 0.1 and 0.2), and they reported that the activation energy for electrical conduction is increased above a certain temperature ($\sim$450 °C). In the low-temperature region, the absolute value of the thermoelectric power is increased by Mg substitution, and the thermoelectric powers of all samples are found to change sign from negative to positive as the temperature increases.

To obtain phonon-glass electron-crystal PGEC materials, the idea of a complex structure, which imagines a material with distinct regions that each provides different functions, has been advanced [35]. Two relatively new material classes are widely regarded as PGEC materials, namely, the clathrates and the filled skutterudites. Clathrates are periodic solids in which tetrahedrally coordinated atoms form cages that surround a metal atom [45]. Clathrate I materials have the general formula A_8E_{46}, with A=Na, K, or Ba and E=Al, Ga, In, Si, Ge, or Sn. Clathrates II and III have idealized formulas of $A_{24}E_{136}$ and $A_{30}E_{172}$, respectively, and exist with the same A and E elements; see Fig. 5 [46]. The low thermal conductivities for semiconducting clathrates are attributed to resonant scattering of the acoustic heat-carrying phonons by the guest atoms. The localized low-frequency vibration mode of the guest atoms is expected to cut through the acoustic branches, which decreases the number of acoustic phonon modes and effectively limits the heat transport [47], i.e., the enhanced vibration of the guest atoms A causes a flattening of the phonons bands, lowering the velocity of the phonons, which significantly contributes to the low thermal conductivity of these materials [46]. However, a few studies have investigated clathrate structures, and all have reported $ZT < 1$ [48].

The essence of the PGEC concept is to synthesize semiconducting compounds in which one of the atoms is weakly bonded in an oversized atomic cage. In this sense, the skutterudite system is a promising material for thermoelectric applications [49]. The basic family of binary semiconducting compounds has been widely investigated; a skutterudite structure generally has the form MX_3, where M is the transition metal element, Co, Rh, or Ir, and X is the pnictogen element, such as P, As, or Sb. Examples of skutterudite structures are CoP_3, $CoAs_3$, $CoSb_3$, RhP_3, $RhAs_3$, $RhSb_3$, IrP_3, $IrAs_3$ and $IrSb_3$ [30]. For several years, efforts have been focused on the preparation and characterization of ternary skutterudites that are isoelectronic to the binary skutterudites [50]. Ternary skutterudites can be obtained either by substitution at the anion site, X, by a pair of elements from groups IV and V (e.g., $CoSb_{3-y}Sn_y$) [51] or by isoelectronic substitution at the cation site, M, by a pair of elements from subgroup VIII (e.g., $Fe_xCo_{4-x}Sb_{12}$) [52]. Binary skutterudites are known for their high electron mobilities and favorable Seebeck coefficients but, unfortunately, have large values of lattice thermal conductivity. Filling the voids with elements that are loosely bound and thus able to "rattle," thereby providing a phonon-scattering mechanism in the skutterudite structure, provides a possible solution to this obstacle [53]. Filling the interstitial voids in the structure with foreign atoms, especially alkaline-earth atoms [54,55], rare earth atoms [56–59] and other ions [60,61], is an effective method of reducing the thermal conductivity while maintaining the electrical conductivity and the Seebeck coefficient of $CoSb_3$-based skutterudites [62]. Many such efforts toward filling skutterudites have been reported: (i) partially filled skutterudite (e.g., $La_{0.1}Co_4Sb_{12}$) [63], (ii) filled skutterudite (e.g., $CeFe_4Sb_{12}$) [64], (iii) double-filled skutterudite (e.g., $Ba_xCe_yCo_4Sb_{12}$) [65] and (iv) multiple-filled skutterudite (e.g., $Yb_{0.2}Ce_{0.15}In_{0.2}Co_4Sb_{12}$) [66]. Meanwhile, filling the core of the cage-like framework, as shown in Fig. 6, via doping [67] can also serve to reduce the thermal conductivity [68]. The substitution of antimony by Se and Te can influence the electronic structure and electrical properties of the material; in particular, such substitution leads to a substantial change in the carrier masses and enhanced scattering of phonons on impurities [69]. Generally, n-type $CoSb_3$ is prepared by substituting Fe, Ni, Pd or Pt into Co sites, which enhances the mass fluctuation scattering [70,71], thereby significantly reducing the lattice thermal conductivity from its original value. However, investigations of filled skutterudite as a promising candidate for power-generation applications in the temperature range of 500–800 K [72] have led to observations of large ZT values for many n-type filled skutterudites, such as 1.3 at 800 K for $Ba_{0.08}Yb_{0.14}Eu_{0.10}Co_4Sb_{12}$ [73] and 1.7 at 850 K for $Ba_{0.08}La_{0.05}Yb_{0.04}Co_4Sb_{12}$ [74].

Among the numerous TE materials, half-Heusler (HH) alloys have attracted considerable attention because of their appealing electrical transport properties and their relatively high Seebeck coefficients in addition to their rich elemental combinations [75]. These alloys have three components that may originate from different elemental groups or may be a combination of elements in the same group. Two of the groups are composed of transition metals, and the third group consists of metals and metalloids.

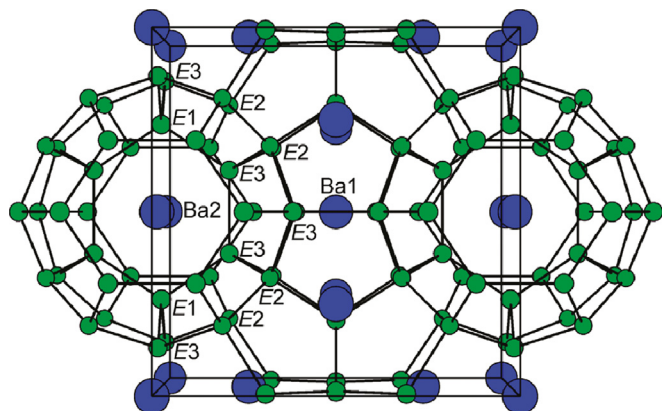**Fig. 5.** Crystal structure of cubic $Ba_8Ga_{16}Si_{30}$. All three E sites are mixed occupied by Ga and Si [46].

Metal Atom (Co, Rh, Ir)
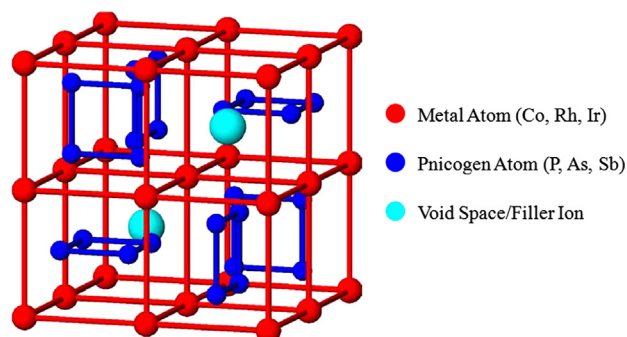Pnicogen Atom (P, As, Sb)
Void Space/Filler Ion

Fig. 6. Crystal structure of filled skutterudite [67].

The chemical formula of half-Heusler alloys is XYZ, where X, Y, and Z can be selected from many different elemental groups (for example, X=Ti, Zr, Hf, V, Mn, or Nb; Y=Fe, Co, Ni, or Pt; Z=Sn or Sb). The crystal structures of the ternary intermetallic compounds usually are of the cubic MgAgAs type (space group F-43m) [76]. Fig. 7 shows the crystal structure of half-Heusler compounds XYZ [77]. These compounds have a narrow band gap on the order of 0.1–0.2 eV at the Fermi level and have garnered interest because of their potential as thermoelectric materials [78]. Their associated large effective masses lead to several characteristics, including large thermoelectric power factors, large Seebeck coefficients ($250\ \mu V\ K^{-1}$) at room temperature, moderate electrical resistivity ($1–10\ \mu \Omega$ m) and high thermal conductivity ($\sim 10\ W\ m^{-1}\ K^{-1}$) at room temperature [79]. MNiSn and MCoSb (M=Ti, Zr, Hf) compounds are of great interest among the half-Heusler family because of their good thermoelectric properties. The state-of-the-art ZT values of MNiSn (M=Ti, Zr, Hf) compounds are close to unity [80]. However, most efforts thus far have concentrated on the optimization of the thermoelectric performance of n-type half-Heusler alloys. The search for promising p-type half-Heusler materials that can be coupled to existing high-performance n-type half-Heusler alloys for high-temperature thermoelectric power generation has only been initiated in the past decade [81].

Typically, metals have been used as dopants. The low-temperature structural phase transitions of Bi-, Pb-, In- and Sn-doped samples of thermoelectric Zn_4Sb_3 have been characterized on crystals grown from molten metal fluxes by Nylén et al. [82], and they observed that when preparing β-Zn_4Sb_3 in the presence of metals with low melting points (Bi, Sn, In, and Pb), the additional metal atoms are unavoidably incorporated in small concentrations (0.04–1.3 wt%), act as dopants and alter the subtle balance between Zn disorder and Zn deficiency in Zn_4Sb_3, which has dramatic consequences for its low-temperature structural behavior.

In general, metals with poor conductivity are good candidates for providing enhanced values of thermoelectric power. It might be important to consider that most metallic materials contain inclusions, which can be either metallic or non-metallic. Inherent to the elaboration process, they are distributed inside the materials. These inclusions in alloys reduce their mechanical strength and resilience, are detrimental to surface finish and increase porosity, and they have a tendency to increase corrosion [83]. Furthermore, they act as stress enhancers and can cause the premature failure of in-service components.

3.2. Ceramics

Over the past two decades, from the discovery of the first ceramic thermoelectric material, many efforts have been put forth to obtain high-performance thermoelectric materials for application in energy-conversion systems [84]. To date, the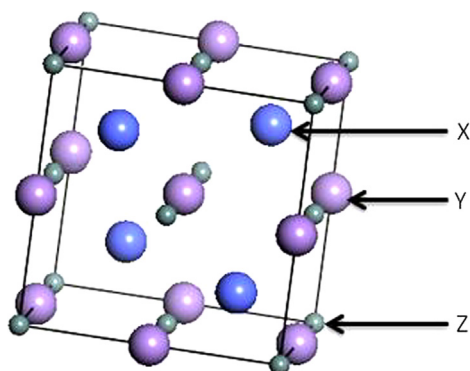 doped alloy TE materials based on Bi_2Te_3 are the best-known ones, and they exhibit $ZT \approx 1$ at room temperature. However, because they are easily oxidized and vaporized, these TE alloy materials cannot be used for applications at high temperatures in air [85]. Therefore, oxide TE materials are used instead at high temperatures and in oxygen. Thermoelectric oxide materials have drawn much attention because of their good thermal stability at high temperatures and their low toxicity compared to conventional intermetallic alloys [86]. However, research seeking efficient thermoelectric materials often involves no conventional semiconductors. In this sense, oxide compounds such as $NaCo_2O_4$, $LaCoO_3$, $(ZnO)_mIn_2O_3$, $BaSnO_3$, $BaPbO_3$, $Ca_3Co_4O_9$, $Sr_{1-x}Nd_xTiO_3$ and $Bi_2Ca_2Co_2O_x$ are promising candidates for thermoelectric materials because of their transport properties and their physical and chemical stability [87–94]. The addition of titanate nanotubes (TNTs) (2 vol%) fabricated via the pressureless sintering method has been found to enhance the ZT value of Nb-doped $SrTiO_3$ polycrystalline ceramic to approximately 0.14 at 900 K [95]. $(Ca_{1-x}Sr_x)_3Co_4O_9$ polycrystalline has been fabricated by using spark plasma sintering method to substitute Ca by Sr, and the result demonstrated that the figure of merit ZT achieves 0.22 at 1000 K for the composition $(Ca_{0.995}Sr_{0.005})_3Co_4O_9$ [96]. However, the fabrication of modules based on oxide materials has only recently begun to emerge, and there exist very few reports concerning the performance of these materials [97]. The oxide nature of the thermoelectric elements and the processing specifications, which involve very high temperatures, make the fabrication a difficult task and different from that of conventional thermoelectric modules [97].

3.3. Polymers

Among the various categories of thermoelectric materials, a great deal of attention has recently been paid to organic TE materials, particularly since the discovery of conducting polymers [98]. In this regard, polymers are very attractive because they are light, flexible, and suitable for room-temperature applications and because they generally require relatively simple manufacturing processes (i.e., spin coating and inkjet printing) compared to semiconductor-based thermoelectrics. Polymers are intrinsically poor thermal conductors, which make them ideal for use as thermoelectrics, but their low electrical conductivity, Seebeck coefficient, and stability have hampered their use in thermoelectric applications [99]. However, compared to inorganic TE materials, organic or polymer TE materials exhibit several inherent advantages, such as potentially low cost because of the abundance of carbon resources, simple synthesis in general, abundant electron-energy bands through modulation, simple processing into versatile forms, high energy density, and low k, which may be of great importance for their potential TE applications. The physical and chemical properties of certain polymers are tunable within a fairly large range of modifications of their molecular structures [100]. The ionic conducting polymers, such as poly (3,4-ethylenedi-oxythiophene):poly(styrenesulfonate) (PEDOT: PSS), which possess high electrical conductivity and intrinsically low thermal conductivity, are considered to be the most promising novel organic TE materials [98]. In a two-component nanocomposite, the selection of a conducting polymer and an inorganic thermoelectric material may yield high thermoelectric power and high electrical conductivity of the material. Because these properties are dependent on the particle size and morphology, it is interesting to map the relation between the structural and electrical properties of the material. Recently, various researchers have attempted to prepare nanocomposites/hybrids/heterostructures of inorganic thermoelectrics with conducting polymers [101]. Table 1 summarizes the electrical conductivity σ, Seebeck coefficient α, thermal conductivity k and power factor PF as well as the highest ZT value of a few typical polymer and polymer–inorganic TE nanocomposites. Du et al. [102] reviewed the

Fig. 7. Crystal structure of the half-Heusler type compounds [77].

Table 1

The electrical conductivity σ, Seebeck coefficient α, thermal conductivity k and power factor PF as well as the highest ZT value of a few typical polymer and polymer–inorganic TE nanocomposites [102].

Materials	σ (S/cm)	α (μV/K)	k (W/mk). Maximum PF (μW/mK^2) or ZT
PANI	$\sim 10^{-7}$–320	~ -16–225	κ, ~ 0.02–0.542 ZT_{max}, 1.1×10^{-2} at 423 K
PANI-inorganic TE nanocomposites	0–-140	~ -30–626	κ, 0.25–1.2
PTH	$\sim 10^{-2}$–10^3	~ 10–100	κ, 0.028–0.17, ZT_{max}, 2.9×10^{-2} at 250 K
PTH -inorganic TE nanocomposites	7.1–8.3	-56–1283	PF$_{max}$, 2.5×10^{-2}
PEDOT:PSS	0.06–945	8–888	κ, 0.34, ZT_{max}, 1.0×10^{-2} at 300 K
PEDOT-Tos	6×10^{-4}–300	40–780	κ, 0.37, ZT_{max}, 0.25 at RT
PEDOT:PSS-inorganic TE inorganic nanocomposites	0–400	~ -125–167	κ, 0.22, ZT_{max}, 0.10 at RT
PPY	0–340	-1–40	κ, 0.2, ZT_{max}, 3×10^{-2} at 423 K
PA	$\sim 1.53 \times 10^{-3}$–2.85×10^{-4}	~ 0.5–1077	
PC	$\sim 4.0 \times 10^{-5}$–5×10^2	4.9–600	PF$_{max}$, 1.9
PMeOPV	46.3	39.1	PF$_{max}$, 7.1
P(ROPV-co-PV)(RO-MeO,EtO and BuO)	183.5–354.6	21.3–47.3	κ, 0.25–0.80 (estimated), ZT_{max}, 9.87×10^{-2} at 313 K
Others polymer–inorganic TE nanocomposites (polymer/carbon nanotube with different contents of CNT	~ 0–48	~ 40–50	κ, 0.18–0.34, ZT_{max}, 0.006 at RT

research progress concerning conducting polymers and their corresponding TE nanocomposites, and their primary focus was TE nanocomposites based on conducting polymers such as polyaniline (PANI), polythiophene (PTH), and poly (3,4-ethylenedioxythiophene): poly(styrenesulfonate) (PEDOT:PSS), as well as other polymers such as polyacetylene (PA), polypyrrole (PPY), polycarbazoles (PC) and polyphenylenevinylene (PPV); these materials appear to have great potential for producing relatively low-cost and high-performance TE materials, and the authors reported that in polymer and polymer–inorganic TE nanocomposites, the value of the Seebeck coefficient typically ranges from -4088 to 1283 μV/K, the electrical conductivity ranges from 10^{-7} to 10^4 S/cm, and the thermal conductivity ranges from 0.02 to 1.2 W/m K. However, it has been demonstrated that the transport properties of conducting polymers are greatly influenced by the process of doping with various materials.

3.4. Semiconductors

Since the late 1950s, research concerning semiconducting thermoelectric devices has been applied for terrestrial cooling and power generation and later for space power generation because of their competitive energy conversion compared to other types of small-scale electric power generators [103]. Semiconductor thermoelectric power generation, which is based on the Seebeck effect, has very interesting capabilities with respect to conventional power-generation systems [104]. During the 1990s, there was a heightened interest in the field of thermoelectrics driven by the need for more efficient materials for electronic refrigeration and power generation. Because of the use of semiconductor materials for thermoelectric applications, there has been a considerable effort to improve the figures of merit (ZT) of these materials to greater than 3 to make them commercially viable. Semiconductor materials are promising for the construction of thermocouples because they have Seebeck coefficients in excess of 100 μV K^{-1} [105], and the only way to reduce k without affecting α and σ in bulk materials, thereby increasing ZT, is to use semiconductors of high atomic weight, such as Bi_2Te_3 and its alloys with Sb, Sn, and Pb. A high atomic weight reduces the speed of sound in the material and thereby decreases the thermal conductivity [106]. A solid-state or semiconductor electronics component, for example, can perform well and reliably for many years when it is operating at or near the ambient temperature [107]. Intermetallic compounds such as Mg_2X (X=Si, Ge, Sn) and their solid solutions are semiconductors with the antifluorite structure and have been proposed as good candidates for high-performance thermoelectric materials because of their superior features such as large Seebeck coefficients, low electrical resistivities, and low
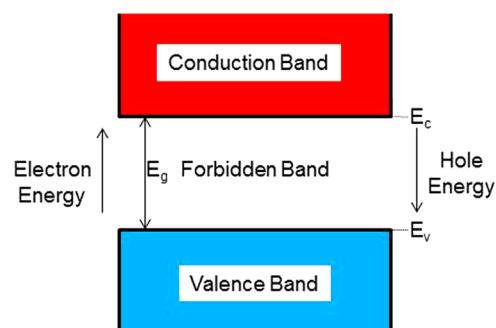

Fig. 8. A simplified energy band diagram of a semiconductor [109].

thermal conductivities [108]. However, the best-ZT materials are found to be heavily doped, small-band-gap semiconductors.

4. Governing parameters for thermoelectric material selection: intrinsic material properties

4.1. Energy gap and band structure in semiconductors

In a solid, electrons exist at energy levels that combine to form energy bands. A simplified energy-band diagram is shown in Fig. 8. The top band is called the conduction band Ec, and the next lower one is called the valence band Ev. The Fermi level Ef (the hypothetical level of potential energy for an electron inside a crystalline solid and a term used to describe the highest of the collection of electron energy levels at a temperature of absolute zero) in intrinsic semiconductors lies essentially halfway between the valence and conduction bands. The region between the valence band and the conduction band is called the forbidden band, where, ideally, no electrons exist [109]. For a conductor such as copper, no forbidden band exists, and the energy bands overlap. For an insulator, conversely, this band is so wide that the electrons require a great deal of energy to move from the valence band to the conduction band. For semiconductors, the gap of the forbidden band is smaller than for an insulator. If the electrons in the valence band are excited externally, they can move to the conduction band. In the valence band, they have an energy of Ev. To move to the conduction band, they require an amount of energy Eg=Ec – Ev, where Eg is the band gap [109].

Since 1954, the control of the energy gap via the effect of the carrier concentration has become one of the methods of greatest interest for controlling the properties of semiconductors. This phenomenon, however, has also been used to analyze the degree of impurity in semiconductor crystals [110]. A great improvement

of electrical properties is closely related to the narrowing of the band gap, though precipitated impurity phases can influence the measured band-gap value [111]. Table 2 lists some semiconducting elements and compounds alongside their band gaps at 300 K [112]. Because electrical transport properties are closely related to the electronic states near the highest valence band and the lowest conduction band for some compounds, it is reasonable to focus on the energy bands near the Fermi level. The band-gap energy is expected to decrease as the atomic number of the constituent atoms increases. The atomic potential spreads more and more as the atomic number increases. This spreading should cause a lowering of the band-gap energy according to two theories that describe these energy bands: the free-electron theory and the tight-binding approximation theory [113]. The Fourier coefficient for the periodic potential should decrease as the overlapping of the atomic potentials increases, and therefore, the band-gap energy should decrease, according to the free-electron theory. However, increasing overlap should cause a larger coupling between neighboring atoms and a broadening of the allowed band, consequently leading to a narrowing of the forbidden band or a decrease of the band-gap energy [114]. When the dispersion of the top valence bands fluctuates within a small energy region, these relatively heavy bands with large effective mass contribute to a high thermopower. For materials with simple band structures, the absolute thermopower value α can be described as follows: C (K_B/e) $\ln(\pi m^* K_B T)^{3/2}/nh^3$ where α is the thermopower, K_B is the Boltzmann constant, e is the elementary charge, n is the carrier density, h is Planck's constant, m^* is the effective mass of the charge carrier, C is an integration constant, and T is the absolute temperature [114]. Ramdas et al. [115] investigated the electronic band gaps of semiconductors as influenced by their isotopic composition, and they reported that isotopically controlled crystals offer an extraordinary opportunity to test theoretical predictions using a variety of spectroscopic techniques.

4.2. Charge carrier concentration

An effective adjustment in the carrier concentration dominates the electronic transport behavior by exerting a significant effect on both the electrical conductivity and the Seebeck coefficient [116]. Furthermore, all thermoelectric properties depend closely on the carrier concentration and typical thermoelectric materials exhibit an optimum carrier concentration of $10^{19} - 10^{21}$ per cm^3 [117]. One of the technologically simplest (and therefore virtually universally used) methods of improving the thermoelectric properties of a semiconductor material is to choose the optimum level of doping,

Table 2
List of some semiconducting elements and compounds together with their bandgaps at 300 K [112].

	Material	Direct/indirect bandgap	Band gap energy at 300 K (eV)
Elements	C (diamond)	Indirect	5.47
	Ge	Indirect	0.66
	Si	Indirect	1.12
	Sn	Direct	0.08
Groups III–V compounds	GaAs	Direct	1.42
	InAs	Direct	0.36
	InSb	Direct	0.17
	GaP	Indirect	2.26
	GaN	Direct	3.36
	InN	Direct	0.70
Groups III–V compounds	α-SiC	Indirect	2.99
	ZnO	Direct	3.35
	CdSe	Direct	1.70
	ZnS	Direct	3.68

where 'optimum' is used in the sense of maximizing the thermoelectric figure of merit. As mentioned above, an optimum electron concentration exists because, as the concentration increases, the conductivity usually increases, accompanied by a simultaneous decrease in the thermopower [34]. Delaizir et al. [118] investigated the p-type alloys $Bi_{1-x}Sb_xTe_3$ with $0.9 \leq x \leq 1.7$, and they observed a linear relation between the amount of antimony, x, and the charge-carrier concentration. The thermoelectric properties and non-stoichiometry of GaGeTe have been studied [119], and the authors reported that the measurement of the transport parameters qualitatively indicated that both $Ga_{1+x}Ge_{1-x}Te$ and $GaGeTe_{1-y}$ are p-type semiconductors ($n \approx 10^{19}$ cm^{-3}). Their hole concentration generally rises with increasing x and y, as demonstrated by the experiment. However, the negative Seebeck coefficient indicates that the transport processes are dominated by electrons as carriers [120]. Thus, the Seebeck coefficient, the electrical conductivity, and the thermal conductivity vary systematically with the carrier concentration [48].

4.3. Mobility

In the presence of several scattering mechanisms, theoretical calculation of the resultant mobility of the charge carriers becomes rather complicated. Until now, no thorough analysis of the validity limits of the common theoretical approaches and adopted models has been performed [121]. Electronic transport is described by the (local) electric-field-induced directional velocity component, v, of the mobile charge carriers (superimposed on their random thermal motion as a time and ensemble average of a fast sequence of acceleration and scattering events), which is associated with a current density $j = e.n.v$, where e is the electric unit charge, and n is the local charge-carrier density. The latter can be altered, in principle, by doping, injection, or photo-generation [122]. The relation between v and the applied electric field E is usually linear for moderate field strengths (reflecting Ohm's law), $v = \mu \times E$ and it is obvious that μ, the charge-carrier mobility, is the fundamental (intrinsic) electronic-transport quantity that is specific to a given semiconductor material [122]. Because the mobility of electrons serves as a direct relation between the crystal structure and the electrical conductivity, the ratio of the mobility μ to the thermal conductivity k is a function of the mean atomic weight. Thus, using the relation for mobility in semiconductors and the Pierls relation for thermal conductivity, we can calculate the ratio as a function of the electron mean free path l_e and the phonon mean free path l_p in a crystal [36]:

$$(\mu/k) = (4e\rho_m l_e)/cv_s(2\pi m_e K_B T)^{1/2} l_p \qquad (5)$$

Here, ρ_m is the mass density; v_s the velocity of sound in the crystal; c is the specific heat of the crystal; and m_e and e are the electron mass and charge, respectively. Using material properties that have been measured for some common semiconductors, the above ratio is plotted against the mean atomic weights of these semiconductors in Fig. 9.

5. Auxiliary properties

5.1. Diffusion properties

Diffusion is the movement of particles from regions of high concentration to regions of low concentration. Diffusion in semiconductors is of great importance for semiconductor technology. As the dimensions of circuits shrink, an understanding of the atom-scale mechanisms of the diffusion processes will become crucial to accurately model and design future devices [123]. In pure (undoped or unalloyed) compounds, the effects of diffusion are not apparent at
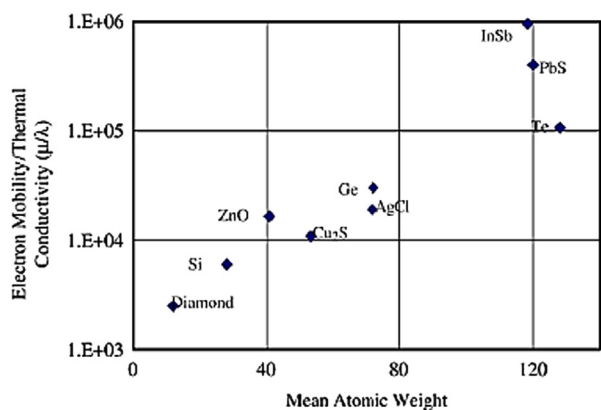
Fig. 9. Ratio of electron mobility to thermal conductivity of thermoelectric materials [36].
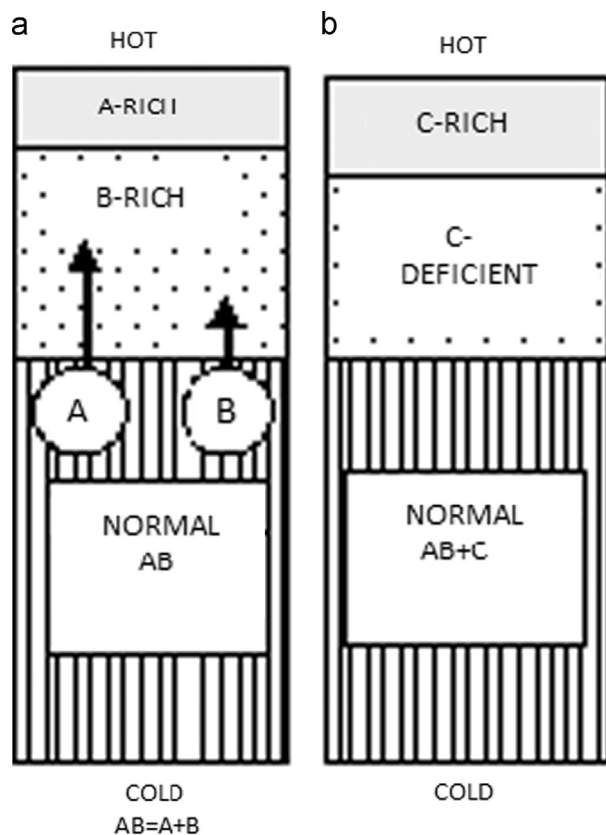

Fig. 10. Effects of diffusion. (a) Unequal rates of diffusion of dissociation products of compound AB results in inhomogeneity. (b) Greater solubility of doping agent C in AB leads to concentration of C at hot end. In both cases, temperature at cold end is insufficient to produce disproportionation [40].

temperatures below that at which the compound begins to dissociate [40]. Once a small amount of dissociation has taken place, however, the products may diffuse at differing rates in the temperature gradients present in the device, and the diffusion of an intentionally added impurity may exhibit similar behavior, as shown in Fig. 10. Self-diffusion in binary compound semiconductors is more complex than in elemental semiconductors because of the larger number of possible native point defects that can, in principle, mediate self-diffusion. In addition to vacancies and self-interstitials on the corresponding sublattices, antisite defects must be considered [124]. Homogeneities in thermoelectric materials are affected by the temperature gradient because the optimal properties can only be obtained within a very narrow temperature region for each homogeneous material, which

greatly limits the efficient utilization of many dispersed energy sources [125]. However, the diffusion effect depends on the band-gap width and the ratio of electron conductivity to hole conductivity. Heavy carrier doping effectively suppresses the diffusion effect, i.e., it inhibits the increase of thermal conductivity at high temperatures.

There have been a number of efforts to characterize defect structures by studying defect-structure-sensitive properties, such as impurity diffusion [126], and many of these efforts have successfully determined diffusion coefficients in semiconductor materials and have also quantitatively analyzed the diffusion process and predicted the results of annealing. Wanwan et al. [127] studied the effect of Cd-diffusion annealing on the electrical properties of CdZnTe and reported that the crystal's resistivity is affected by annealing, which limits diffusion. The nature of this treatment is a diffusion process. Thus, it is meaningful to relate the change in resistivity to the diffusion parameters. The undesirable diffusion of thermoelectric materials when placed in a thermal gradient will result in non-homogeneous and inferior materials, and the importance of diffusion processes is evident at temperatures of approximately 80–90% of the absolute melting point of the materials. A micro-thermoelectric device consists of a bonding layer, electrodes and thermoelectric thin films. At the interfaces between the metallic electrodes, solder materials and thermoelectric thin films in a micro-thermoelectric device, diffusion occurs and degrades the performance and reliability of the device. Thus, a Ni layer is used as the diffusion barrier in some commercial devices that use bulk thermoelectric materials [128]. However, because of undesirable and unpredictable diffusion phenomena, modern process technologies try to reduce diffusion by decreasing the thermal range experienced by the device during operation.

5.2. Oxidizability

For want of a better term, the tendency of the composition of a thermoelectric material to become altered when exposed to the oxygen in the air may be called "oxidizability." As is well known, oxygen is a reactive gas. When oxygen is introduced during deposition, highly energetic atomic ions ejected from the target may react with the oxygen ions via collisions and transform into oxides on the target surface. As the oxygen partial pressure increases, the collision probability between the reactive gas and the atomic ions increases, causing the sputtering and deposition rates to decline [129]. The results of this undesirable phenomenon take two: in one type, a thin surface layer of oxidized material is formed, and the deposition process is inhibited by its formation; the other form involves the diffusion of oxygen into the interior of the material and is therefore progressive [40]. Thus far, oxides have been regarded as unsuitable for thermoelectric applications because of their poor mobility, but some years ago, Terasaki et al. [130] found that a single crystal of the layered cobalt oxide $NaCo_2O_4$ exhibits high thermoelectric performance. Recently, several electrically conductive oxide systems have been recognized as potential candidates for thermoelectric materials; these thermoelectric oxides can be used at high temperatures with no deterioration of their performance caused by oxidation, and their production costs are comparatively low [131]. Zhou et al. [132] investigated the effects of the annealing atmosphere on thermoelectric signals from ZnO films, and they suggested that ambient oxygen plays an important role in the electronic properties of ZnO films. Of p-type transparent semiconducting oxide (TSO) materials, Cu_2O is one of the most promising candidates, and because of the effect of the oxygen flow rate during deposition on the properties of Cu_2O films, the oxygen flow rate must be kept low to avoid the over-oxidation of Cu_2O to CuO and to ensure a non-oxidized/non-poisoned metallic copper target in the reactive sputtering environment. The proper control of the amount and flow rate of

oxygen during deposition can produce good-quality p-type transparent Cu_2O films with electrical resistivities ranging from 10^2 to 10^4 Ω cm, hole mobilities of 1–10 cm^2/V s, and optical band gaps of 2.0–2.6 eV [133]. The synthesis and post-annealing effects on the transport properties of thermoelectric oxide $(ZnO)_mIn_2O_3$ ceramics have been studied by Wang et al. [92], and they inferred that the oxygen defects or vacancies in the InO_2 layers play an important role on both the electrical and thermal transport properties of these $(ZnO)_mIn_2O_3$ ceramics. It has also been reported that the resistivity, carrier concentration, and Hall mobility of Z_5IO films depend strongly on the annealing temperature and ambient atmosphere. Measurements of the Seebeck coefficient and electrical resistivity are most likely among the most sensitive means for the detection of small amounts of diffusive oxidation [40]. However, in some of the most-studied compounds, traces of diffusive oxidation that are visually and chemically undetectable can so severely affect the Seebeck coefficient as to change its sign, and the resistivity can be increased by several decades as a result of this process.

5.3. Brittleness

At low temperatures ($T < 200$ K), single crystals of the Bi–Sb alloys exhibit the best thermoelectric performances, but the brittleness of the single crystals is a problem in practical devices. To ameliorate this limitation, some efforts have been devoted to studying the influence of the growth parameters on the mechanical properties of such alloys [134]. However, the requirements for producing nanostructured TE materials are two-fold: improve their mechanical properties (reduce brittleness and improve machining) and improve their TE properties (figure of merit) [135]. Moon et al. [136] prepared p-type Te-doped Bi_2Te_3–Sb_2Te_3 compounds using rapid solidification and spark plasma sintering (SPS) techniques, and they reported that the solidified powders consisted of homogeneous thermoelectric phase and that as the SPS temperature increases, the microstructure becomes coarser, resulting in a reduction of the hardness. At present, rapid solidification processes (RSPs) such as gas atomization and melt spinning have been reported to offer a novel opportunity for modifying the intrinsic brittleness and thermoelectric anisotropy of Bi–Te-based thermoelectric materials by forming a fine-grained and homogeneous microstructure [137]. One reason for the broad interest in hardness (H) testing is that the microstructure (and hardness) of materials can change dramatically with alloying, and the machinability of brittle materials also has been correlated with hardness. Thus, the compositional dependence of H is significant because H is related to other mechanical properties. For LAST (lead–antimony–silver–tellurium), the fabrication of thermoelectric (TE) modules for waste-heat recovery will require the machining of perhaps several hundred (or more) individual TE legs. Because machinability and wear resistance are functions of H for other brittle materials [138], Zhou et al. [139] investigated the thermal stability and elastic properties of Mg_2X (X=Si, Ge, Sn, Pb) phases from first-principle calculations and calculated the bulk moduli B, shear moduli G, Young's moduli E and Poisson ratios v; they reported that Mg_2Si, Mg_2Ge, Mg_2Sn and Mg_2Pb are all brittle.

5.4. Compression and shear strength

The average strength (the mean of the strength distribution) and Young's modulus (which characterizes the stress–strain response of a brittle material prior to fracture) are fundamental to understand the mechanical properties of a TE material in a practical device [140]. Enhancement of the mechanical strength of a TE module will render it more robust. The largest improvement must be in the shear strength, which is the weakest point of many

TE modules. The compressive strength also must be increased, especially near the perimeter of the module. Such additional compressive strength will be especially useful in preventing damage to the module if, during the assembly process, clamping forces are accidentally applied unevenly to the module. Not only does the brittleness of the material limit the resistance of the device to mechanical and thermal shocks, but the cutting and fabrication of the arms themselves require that the materials used not be too brittle. Hong et al. [141] studied the thermoelectric properties of novel n-type 95% Bi_2Te_2 5% Bi_2Se_3 alloys by gas atomizing and extrusion process, and they reported that the compressive strengths of the compounds hot extruded at 16:1 and 25:1 were 160 and 160 MPa, respectively. The figures of merit Z of the compounds extruded at 16:1 and 25:1 were 2.50 and 2.07×10^{-3} K^{-1}, respectively, because of the different grain sizes induced by the differences in deformation caused by varying the extrusion ratio. The shear strength of aged $CoSb_3$/Ti/Mo–Cu TE joints has been investigated [142], and the results indicated the joints possessed sufficient strength after aging at 575 °C for 720 h. Moreover, the $CoSb_3$/Ti/$W_{80}Cu_{20}$ elements exhibit sufficient shear strength and good electrical contact for the reliability of a thermoelectric device [143]. Experiments conducted by Zhao et al. [144] on nanostructured materials, such as nanoparticles, nanowires, nanotubes, nanopillars, thin films, and nanocrystals, have revealed a host of "ultra-strength" phenomena, which are defined by the stresses in a material component generally increasing to a significant fraction ($> 1/10$) of its ideal strength – the highest achievable stress of a defect-free crystal at zero temperature. However, while thermoelectric modules exhibit relatively high mechanical strength in the compression mode, their shear strength is comparatively low.

5.5. Coefficient of thermal expansion (CTE)

Thermal expansion is critical, as devices for high-temperature applications will be subjected to extreme temperature fluctuations. This property, defined as the fractional change in length or volume with a unit change in temperature, affects several aspects of the design of thermoelectric devices. Generally, the thermal expansion coefficient α ($\alpha = (\Delta L/L_0)/(T_2 - T_1)$) varies inversely with the melting temperature (T_m), and it has been empirically confirmed that the product αT_m is a constant for many substances. This means that a material with high T_m should exhibit low α [145]. The CTE of TE materials is of critical importance because the shear stress is proportional to the temperature gradient, and the larger the heterogeneity in the thermal expansion coefficient of a material is, the larger is the shear stress that will result [146]. Al-Merbati et al. [147] examined the influence of device geometry on thermal stress, thermal efficiency and output power, and the result indicated that the presence of high stress can be attributed to the mismatch of thermal expansion coefficients between the pin and the hot plate, which generates high stress levels at the interface between the hot plate and the pin. With respect to the space group (in mathematics and geometry, a space group is a symmetry group, usually for three dimensions, that divides space into discrete repeatable domains), the Pnma phase exhibited a small but significant decrease in thermal expansion with increasing dopant levels, while the Imma phase exhibited no significant change in CTE with increasing dopant levels. However, these values can be considered representative of the behavior of a bulk polycrystalline sample because of the independence of the thermal expansion from microstructure and porosity [148]. Tachibana and Fang [149] estimated the thermal stress to investigate the reliability of thermoelectric devices by devices via temperature-cycling tests, and they claimed that it was obvious that the thermal stress was determined by the temperature difference, coefficients

of thermal expansion, die height, die cross section, substrate size and so on. However, no explicit relations among these parameters were given. Rogl et al. [150] investigated the effects of high pressure torsion (HPT) processing on the structural, thermoelectric and mechanical properties of $Sr_{0.07}Ba_{0.07}Yb_{0.07}Co_4Sb_{12}$, and they reported that the thermal expansion coefficient below room temperature after processing was slightly lower than before HPT. The thermal expansion of the sample was measured above room temperature both parallel and perpendicular to the pressing direction, and interesting results were obtained: the thermal expansion coefficient calculated for the temperature range of 600–700 K was the same as for the low-temperature region, but the expansion behavior from room temperature to 550 K differed between the first and third measurements and requires further investigation. As the temperature increased from 300 to 550 K, the length first reached a maximum and then was observed to decrease.

6. Applications

Thermoelectric (TE) modules comprise arrays of thermoelectric (TE) junctions, which are connected electrically in series and thermally in parallel. The TE junctions, in turn, consist of p- and n-type thermoelectric materials, which are selected from the range of materials discussed so far in this review, based primarily on their physical thermoelectric performance. Auxiliary to the basic array of TE modules are components that contribute to the overall efficiency of the module, such as heat sinks, which absorb heat from the hot side, and cooling fins or cooling systems, which dissipate heat from the cool side. Typically, a single module may produce power in the range of 1–125 W and may be modularly connected to produce power up to ∼5 kW. The maximum temperature gradient between the hot and cold side can be as high as 70 °C [13]. The general TE module architecture is shown in Fig. 11. Given the nature of TE modules as solid-state devices with no

Fig. 11. Schematic of atypical thermoelectric device [9].

moving parts, they are durable and reliable, with over 100,000 h of operating lifetimes, and have a simple structure. They may operate in two modes: as thermoelectric generators (TEGs), generating electricity from a temperature gradient, or as thermoelectric coolers (TECs), converting a direct current into a temperature gradient [151].

6.1. Applications of thermoelectric devices as coolers

Thermoelectric coolers, which are commonly known as Peltier coolers, have been successfully commercialized for high-performance, niche cooling systems that require high heat-flux dissipation to a very low temperature at a precise rate. These Peltier coolers are well suited for such applications, for which a conventional air-cooling system is no longer adequate to remove the heat fluxes at a sufficiently high rate. The general design criteria for these TECs include high reliability, flexibility in packaging and integration and low weight [152,153].

6.1.1. Cooling electronic devices

In electronic cooling applications, a thermoelectric cooler (TEC) serves as a device for transporting heat away from a surface that has a temperature higher than the ambient temperature. The purpose of a TEC is to maintain the junction temperature of an electronic device below a safe temperature by pumping heat away from the device [152]. A significant increase in both microprocessor power dissipation and CPU size has resulted in an increase in heat fluxes. As a result of the increasing miniaturization of electronic circuitry, microprocessor heat fluxes have also increased and are expected to exceed 100 W/cm^2 for many commercial applications [153]. The development of thermoelectric coolers (TECs) in combination with air cooling or liquid cooling approaches has been of major thermal benefit because a negative temperature gradient and, therefore, a reduced thermal resistance can be generated with the use of a TEC. Fig. 12 illustrates air-cooling techniques (in which a fan is simply added to blow air through the enclosure that houses the electronic components to enhance the heat transfer) for high-power electronic packages such as processors [154]. In addition, TEC applications have been studied for hot-spot thermal management. To aid the design and analysis of these TECs, intensive modeling work concerning the
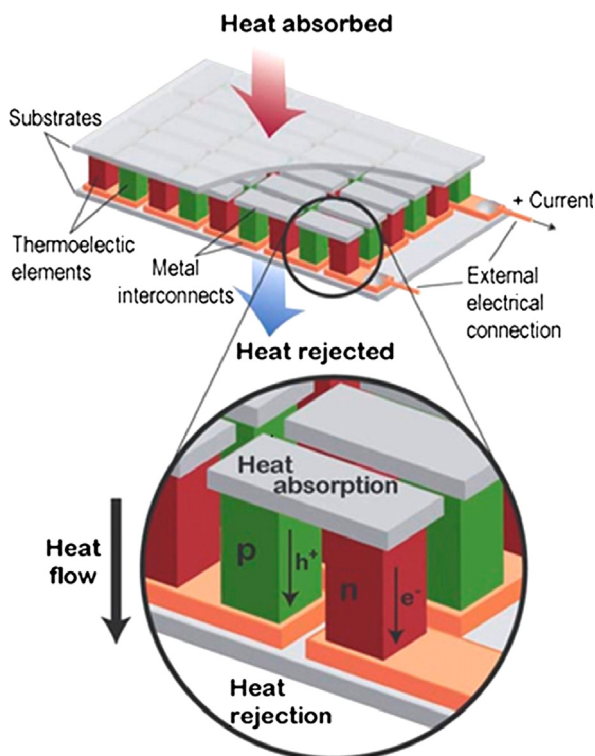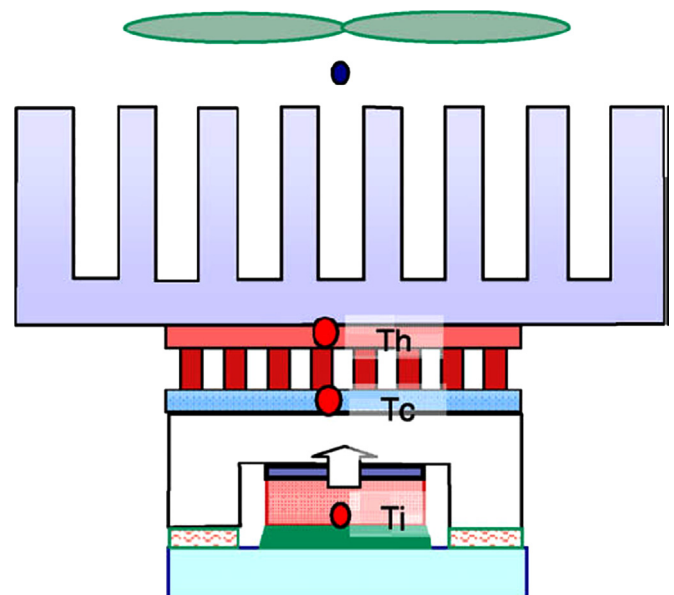

Fig. 12. Schematic of the TEC cooling of a processor with an air cooled heat sink at the top [154].

performance of TECs has been carried out, such as that for the material Bi_2Te_3 [155]. Chang et al. [156] developed a theoretical model of a thermal analogy network to predict the thermal performance of a TEC with an air-cooling module. They reported that at a specific heat load, the TEC air-cooling module achieves its best cooling performance at an optimum input current between 6 A and 7 A and for heat loads between 20 W and 100 W. Their result also demonstrated that the thermoelectric air-cooling module performs better at a lower heat load. Similarly, Huang et al. [157] demonstrated experimentally that the thermal performance of a conventional water-cooling device can be effectively enhanced by integrating it with a thermoelectric cooler when the heat load is below 57 W. Zhou and Yu [158] conducted detailed analyses of the optimal allocation of the finite thermal conductance between the cold-side and hot-side heat exchangers of a TEC system. The analysis results when the constraint of the total thermal conductance was considered demonstrated that the maximum coefficient of performance (COP) can exceed 1.5 when the finite total thermal conductance is optimally allocated. However, overall, the efficiency of the hot-side heat exchanger parameters is usually the predominant factor in determining the overall performance of a TEC system [158,159].

6.1.2. Refrigerators and air conditioners

In refrigeration applications for which cost is not the main criterion, Peltier cooling appliances provide rapid cooling; a solar Peltier refrigerator may reduce the temperature from 27 °C to 5 °C in approximately 44 min [160]. A thermoelectric refrigeration system, which has the merits of being light, reliable, noiseless, rugged, and low cost in mass production, uses the charge carriers in the thermoelectric material rather than refrigerant as the heat dissipation carrier [161]. One attractive application is for outdoor purposes, when operated in tandem with solar cells, as shown in Fig. 13. In the daytime, solar cells receive solar energy and turn it into electric power supplied to the thermoelectric refrigerator by means of the photovoltaic effect. If the amount of electric power produced is sufficient, the power surplus can be accumulated in a storage battery in addition to driving the refrigerator. If the solar cells cannot produce sufficient electric power, for example, on cloudy or rainy days, the storage battery may serve as a supplementary power source, and it can be used to power the

Fig. 13. Schematic of solar cell driven, thermoelectric refrigerator (prototype) [161].

refrigerator at night. Although the coefficient of performance of such a system is not as high as for a vapor-compression cycle [161], thermoelectric refrigerators have been used in military, aerospace, instrument, and industrial or commercial products as cooling devices for specific purposes; for example, TEC systems, when used as microclimate cooling (MCC) systems, can remove a significant amount of heat from a soldier's body while he or she is wearing combat clothing, thus increasing mission duration and enhancing mission performance [162]. Luo et al. [163] investigated the cooling potential of bulk single-phase $Bi_{85}Sb_{15}$ material. This material, which was prepared via melt spinning (MS) combined with a subsequent spark plasma sintering (SPS) technique, provided an optimized power factor of 7.9 mW/mK^2 for the sample with the highest cooling rate. Meng et al. [164] conducted numerical studies of the cooling load and coefficient of performance of a commercial water-cooling thermoelectric refrigerator with a maximum cooling load of 2.33 W and a maximum COP of 0.54. The results demonstrated that the heat convection of the heat exchanger and the heat leakage through the air gap are the main factors that can cause irreversibility and decrease the performance of the system. The COPs of present commercial thermoelectric refrigerators (for example, Melcor's Polar TEC^{TM} series of thermoelectric devices) are typically between 0.3 and 0.7 for single-stage applications. Moreover, COPs greater than 1.0 can be achieved when the module is removing heat from an object that is warmer than the ambient temperature [165].

Thermoelectric air conditioners (TEACs) are environmentally friendly, simple and reliable; they offer convenient installation and support complex water distribution pipes, and switching between the cooling and heating modes can be easily achieved by reversing the input current. However, these systems are still very expensive at present [166]. TEACs are portable and low noise, but they have a relatively low COP, which is an additional factor that limits their application for domestic cooling. TEACs, however, have a large potential market as air conditioners for small enclosures, such as cars and submarine cabins, where the power consumption would be low or safety and reliability would be important [167]. For example, Cherkez [168] theoretically determined the maximum coefficient of performance (COP) of an air conditioner based on a permeable thermoelectric converter. Considering the optimal structural and thermophysical parameters, including the applied electrical current and the heat-carrier velocity in the channels of the thermo-elements, the results indicated the possibility of increasing the COP by a factor of 1.6–1.7.

6.2. Application of thermoelectric devices for power generation

Thermoelectric generators (TEG), in principle, may offer many advantages over conventional electric-power generators, such as being highly reliable, silent in operation, and environmentally friendly and containing no moving parts [169]. Because of these advantages, considerable emphasis has been placed on the development of TEGs as a standalone power-generation technology for a variety of aerospace, biomedical, remote power and military applications [13].

6.2.1. Low power generation

Body-mounted electronic devices may be broadly categorized into those intended for mobile communications purposes, such as smartphones, MP3 players and iPods, and those for medical purposes, such as hearing aids and cardiac pacemakers. The power requirements of these body-mounted devices range from 5 μW to 1 W, with a corresponding life expectancy of up to 5 years, indicating a need for an energy source that is both portable and autonomous [170]. Today, batteries represent the dominant energy
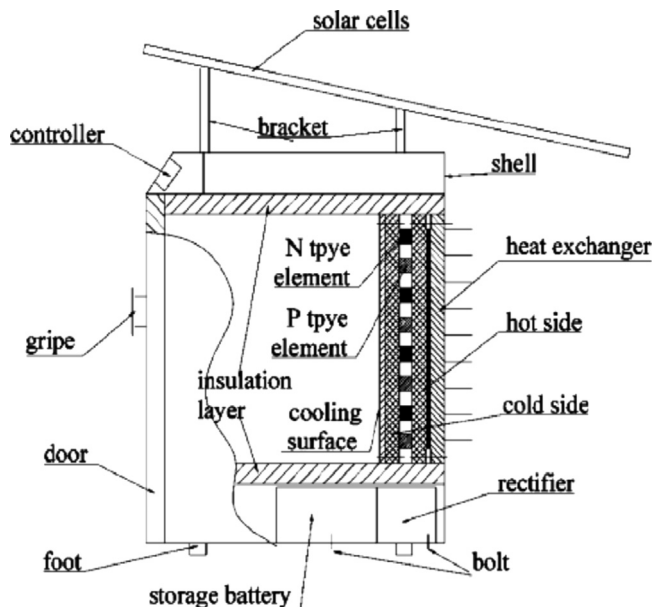
source for portable devices. Although the energy density of batteries has increased by a factor of 3 over the past 15 years, in many cases, their presence has had a large impact on, or even dominated, the overall size and operational cost of portable devices [170]. Furthermore, batteries contain chemical substances or materials that are harmful to the environment, such as sulfuric acid, mercury, zinc, lithium, lead, nickel and cadmium, and exhibit toxicity that can cause damage to humans and the environment. For this reason, body-mounted TEGs are an attractive proposition, as they may be fabricated out of safer materials than Ni-Cd or lithium-ion batteries [13]. So far, a thermoelectric wristwatch that is driven by body heat has appeared as one commercialized example of body-mounted TEGs. Two known manufacturers of these TEG wristwatches are Seiko and Citizen; the Seiko watch typically produces 300 mV of open-circuit voltage from a temperature gradient of 1.5 K, and its efficiency is approximately 0.1% [171].

6.2.2. High power generation

(a) Waste heat thermoelectric generators: Traditionally, large-scale electricity generation is achieved via the burning of fossil fuels (e.g., heat engines) or from nuclear or hydropower sources. Each of these technologies has some disadvantages in terms of environmental impact. For example, the burning of fossil fuels has been linked to environmental pollution and global warning, while nuclear electricity carries a risk of nuclear meltdown, as demonstrated by the 2011 Fukushima disaster. TEGs circumvent these problems, as they generally offer a low environmental risk. Furthermore, TEGs are an intelligent way of mitigating the adverse effects of global warming, as they are able to generate electricity by harvesting waste heat, such as heat that is the byproduct of industrial processes, such as the steelworks industry, and automobile engines. Recognizing the potential of waste heat as an energy resource, these two industries have been the main driving force behind the development of commercial TEGs for high-power electricity generation. The energy-conversion efficiency of a TEG (η_{te}) is determined by both the operating temperature of the generator and the unitless figures of merit (ZT) of the thermoelectric materials used, as follows:

$$\eta_{te} = ((T_h - T_c)/T_h).(\sqrt{(1+ZT)} - 1)/(\sqrt{(1+ZT)} + T_c/T_h) \qquad (6)$$

where T_h is the hot-side temperature, and T_c is the cold-side temperature; these temperatures are selected based on the application of the TEG. Komatsu's Bi_2Te_3-based thermoelectric generator, touted as the world's most efficient, has $\eta_{te} = 7.2\%$ and produces an output density of approximately 1 W/cm^2 when operating at $T_c = 30$ °C and $T_h = 280$ °C [172]. In the case of waste-heat-recovery power generation, several leading automobile manufacturers, such as Volkswagen, Volvo, Ford and BMW, have been developing TEG waste-heat-recovery systems to improve the fuel economy of their automobiles with potential power generated from the TEGs in the range of ~1 kW. Even despite the currently low TEG efficiency, diligent harvesting of waste heat from resources such as automobile exhaust via judicious design and fabrication methods and maintenance strategies render TEGs a worthwhile technology for investment by these automobile manufacturers [171]. A TEG with a ZT of 1.25 and an efficiency of approximately 10% could be used to harvest 35– 40% of the energy from the exhaust manifold, which has an average temperature of 250 °C, to generate useable power that would contribute directly to the operation of the equipped vehicle, which could increase fuel efficiency by up to 16% [173]. Most of these automobile TEGs use BiTe-based bulk thermoelectric materials, as an optimal ZT in the temperature range < 500 K may be achieved using this compound, and therefore, the manufacturing processes for this compound have been extensively developed.

Table 3
The characteristic of available thermoelectric generator materials [15].

Temperature (°C)	Type	TEG materials	ZT (maximum)
< 150	p	Bi_2Te_3	0.8
	n	Bi_2Te_3	0.8
150–500	p	Zn_4Sb_3	–
	p, n	PbTe	0.7–0.8
	p	TeAgGeSb(TAGS)	1.2
500–700	p	$CeFe_4Sb_{12}$	1.1
	n	$CoSb_3$	0.8
700–900	p, n	SiGe	0.6–1.0
	p	LaTe	0.4

Table 3 presents the characteristics of available thermoelectric generator semiconductors [15]. Hsu et al. have designed a system for the recovery of waste heat that comprises 24 TEG modules to convert heat from the exhaust pipe of an automobile to electrical power [174]; a temperature difference of 30 °C was able to produce a total power output of 12.41 W. In another development effort, Karri et al. [175] simulated a performance comparison of a TEG containing bismuth telluride (Bi_2Te_3) and quantum-well (QW) thermoelectric materials. The TEGs containing these two materials were placed in the exhaust streams of a sports utility vehicle (SUV) and a stationary, compressed-natural-gas-fueled engine generator set (CNG). The results predicted an increase in power between the QW- and Bi_2Te_3-based generators of approximately a factor of three for the SUV and a factor of seven for the CNG generator under the same simulation conditions. The relative fuel savings for the SUV averaged approximately –0.2% using Bi_2Te_3 and 1.25% using the QW generator. For the CNG case, the fuel savings was approximately 0.4% using Bi_2Te_3 and approximately 3% using the QW generator. However, any temperature fluctuation on the hot side leads to a rapid change in the output power generated by the TEG, which is dangerous to electric devices [176].

While the energy conversion efficiency is a useful metric for considering the performance and selection of TEGs, the cost of generating electricity is of comparatively equal importance for the development of commercial devices. For practical applications, the cost of power generation – as governed by material, manufacturing, and heat-exchanger costs – is a critical factor that is not captured by the figure of merit, ZT, alone [177]. Komatsu, which boasts the world's highest-efficiency TEG module, in their technical report by Sano et al. [178], deduced that the selling prices of Bi–Te-based thermoelectric modules range from $7 to $42 per watt at a maximum energy-conversion efficiency of 15%. Consequently, current applications of TEGs are restricted to niche sectors where reliable power generation is required irrespective of cost and efficiency, such as deep-space missions and oil and gas platforms.

(b) Solar thermoelectric generators (STEGs): Solar thermoelectric generators (STEGs) were initially designed and optimized for space applications because of their advantages of reliability and long lifetimes as well as their ability to capture high levels of incident solar radiation in extraterrestrial regions; however, much of the recent interest in these systems has been focused on residential solar-thermal-energy harvesting [1,179–185]. The STEG may be described as consisting of a TEG and a thermal collector. Solar heat can be absorbed by the thermal collector and then concentrated and conducted over the thermoelectric generator using a fluid pipe or some other means. Subsequently, the thermal resistance of the thermoelectric generator will lead to a temperature difference that is proportional to the heat flux from the absorber of the thermal collector to the fluid. As a result, electric power will be generated by the thermoelectric generator, and this power will be proportional to the temperature difference [1]. Suter et al. [181] simulated a 4-leg TEC module consisting of two pairs of

p-type $La_{1.98}Sr_{0.02}CuO_4$ and n-type $CaMn_{0.98}Nb_{0.02}O_3$ legs sandwiched between two ceramic Al_2O_3 hot/cold plates and exposed to concentrated solar radiation. The heat-transfer analysis for the module indicated that a large amount of solar heat is lost in such STEGs: more than 70% of the incident solar power was lost to re-radiation and free convection from the absorber, while 20% was conducted through the legs, and $<10\%$ was lost via radiation to the cold plate, resulting in a maximum efficiency of only 0.081%. Further experimental and analytical improvements to overcome these thermal losses were achieved by He et al. [182], who incorporated thermoelectric modules with glass evacuated-tube heat-pipe solar collectors (SHP-TE). The simulation results indicated that the evacuated-tube heat-pipe solar collectors had a significant effect on the TEG by increasing the thermal efficiency by approximately 55%, which may increase the performance to above 1%. Meanwhile, Kraemer et al. [183] predicted a peak efficiency of 5 with a thermoelectric material cost of below 0.05 $/W_p$ by modeling an optimized methodology for terrestrial solar thermoelectric generators (STEGs). Miljkovic and Wang [186] modeled and optimized a novel hybrid solar thermoelectric (HSTE) system that uses a thermosyphon to passively transfer heat to a bottoming cycle to determine the overall performance in a temperature range of 300–1200 K for solar concentrations of 1–100 suns and various thermosyphon and thermoelectric materials with a geometry resembling an evacuated-tube solar collector. Bismuth telluride, lead telluride, and silicon germanium thermoelectrics were studied with copper/water, stainless-steel/mercury, and nickel/liquid-potassium thermosyphon/working-fluid combinations. The system contained a parabolic trough mirror that concentrated solar energy onto a selective-surface-coated thermoelectric to generate electrical power, and a thermosyphon adjacent to the back side of the thermoelectric maintained the temperature of the cold junction and carried the remaining thermal energy to a bottoming cycle; see Fig. 14. This HSTE system demonstrated that ideal efficiencies as high as 52.6% can be achieved at a solar concentration of 100 suns and a bottoming-cycle temperature of 776 K. However, the performance of a solar thermoelectric generator is primarily limited by the thermoelectric materials used to construct it; bismuth telluride is a favorable low-temperature thermoelectric material that exhibits advantageous properties and can reaches a maximum of $ZT \sim 1$ at low temperatures in the range of (25–225 °C), while filled skutterudite is a good medium-temperature thermoelectric material that can be operated over a wide temperature range (25–525 °C) [184]. Moreover, the total conversion efficiency for solar energy of a solar thermoelectric generator based on a multi-stage thermoelectric module could be as high as 10%. With the continuous emergence of new thermoelectric materials, solar thermoelectric generators using multi-stage and hybrid-generation-system (HGS) thermoelectric modules will have good application prospects [184,185].

6.3. Applications of thermoelectric devices as thermal-energy sensors

Many new types of thermal-energy sensors based on the Peltier effect or Seebeck effect of thermoelectric modules have been developed in the last two decades, such as sensors for power ultrasound effects [187], cryogenic heat-flux sensors [187,188], water-condensation detectors [189,190], fluid-flow sensors [191–193], and infrared sensors [194–199]. These sensors generally rely on the conversion of heat into electrical signals or vice versa.

Infrared (IR) sensors, which operate on the principle that any mass radiates heat, allow the detection of heat using the Seebeck effect; the absorption of heat causes a specific temperature rise, which subsequently produces a Seebeck voltage. The main sensor parameters are the responsivity, which is given by the ratio of the sensor voltage to the incoming radiation power; the time constant; and the noise voltage [194,195]. Hirota et al. [196] developed a low-cost thermoelectric infrared sensor (thermopile) using polysilicon with a precisely patterned Au-black absorber that provides a high responsivity of 3900 V/W and a low cost potential. However, most thermoelectric IR sensors are able to operate in the range of 7–14 μm.
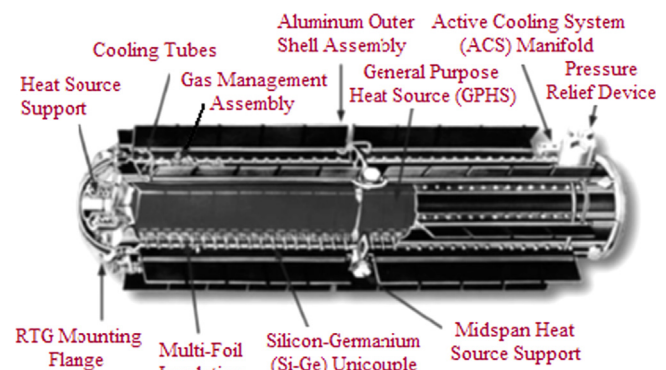

Fig. 15. Current RTGs with 18 GPHS modules and SiGe thermoelectric unicouples for generating 280 W_e at beginning of life ($\sim$5.5 W_e/kg) [205].
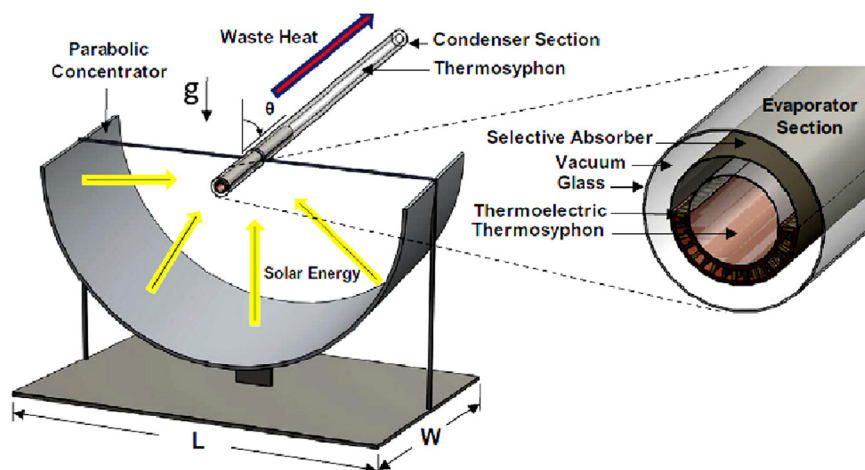

Fig. 14. Schematic of the hybrid solar thermoelectric system (HSTE). Solar energy is focused by a parabolic concentrator on the evaporator section of the evacuated tube absorber (thermosyphon), which heats the TE hot side. The resulting temperature difference between the TE hot and cold sides produces electrical power while heat carried away (waste heat) by the thermosyphon (adjacent to the cold side) is transferred to the condenser section for the bottoming cycle [186].

Kopparthy et al. [200] developed a thermoelectric microfluidic sensor (TMS) for biochemical applications. The device consists of a 100 μm deep microfluidic channel with a Bi/Sb thin-film thermopile attached to its bottom surface. The device has a sensitivity of 0.045 V s J^{-1} when known quantities of energy are applied to a nichrome heater incorporated on the inner side of the bottom wall of the microfluidic sensor bottom channel wall, while continuously injecting deionized (DI) water. Using the Seebeck and Peltier effects Stachowiak et al. [191] developed a fluid-flow sensor for use in the low-velocity range. This sensor, when placed in a typical cylindrical duct of 100 mm in diameter, produced an output signal of 185 μV for a fluid-flow range from zero to 1.5 m^3/s with a maximum error of $\pm$ 4%. A sensor system combining a novel pressure-stable thermoelectric flow and an impedimetric sensor for monitoring chemical conversion in microfluidic channels was developed by Jacobs et al. [192]. Both sensor chips were optimized for hydraulic diameters of ~1 mm and exhibit a high chemical, temperature and pressure stability. However, in terms of size and light weight, the most effective structure for thermoelectric sensors is the thin-film structure [201,202].

6.4. Aerospace applications

Advanced autonomous power systems that can be operated continuously and independently of the sun and are capable of providing electric power from a few watts to hundreds of kilowatts for 7–10 years are required for extraterrestrial exploration vehicles. For example, the solar brightness on Mars and Jupiter is as weak as 45% and 4%, respectively, and it is negligible on other planets. As a result, the solar option is suitable only for robotic and spacecraft missions that are limited in their time scope of operation and require only a few watts of electrical power (~10 W) [203]. Radioisotope thermoelectric generators (RTGs) have been used by the United States to provide electrical power for spacecraft since 1961. The required electrical output power levels can be achieved by the appropriate selection of a number of general-purpose heat-source (GPHS) modules incorporated in an RTG system. A GPHS module is a composite carbon body that houses a total of four fuel pellets and acts as an aero-impact shell. The isotope fuel for the GPHS-RTG is in the form of plutonium dioxide (^{238}PuO$_2$) at approximately 80% density. For power conversion by the GPHS-RTG, thermoelectric junctions have been used, such as SiGe junctions [204]. SiGe unicouples partially convert the heat generated by the radioactive decay of ^{238}Pu in the ^{238}PuO$_2$ fuel pellets that are encapsulated in the general-purpose heat-source (GPHS) modules [205], as shown in Fig. 15. Previously, lead telluride was used as the thermoelectric converter for lower-powered RTGs operated at a maximum hot junction temperature of < 865 K to produce a power of ~2.7 W$_e$ [206]. Because of the deleterious effects of oxygen on these materials [207], silicon-germanium thermoelectric elements were later adopted for high-powered RTGs operated at high temperatures of up to 1275 K [206]. Their sublimation rates and oxidation effects, even at these higher temperatures, can be controlled by the use of sublimation barriers around the elements and an inert cover gas within the generator during ground operation [207]. In 1976, the Lincoln Experimental Satellite (LES) 8/9 was the first spacecraft to use the new "> 150 W$_e$ multi-hundred watt (MHW) RTG," which employed 312 SiGe-alloy thermoelectric elements per RTG [208].

Recently, skutterudite alloys with *ZT*s ranging from ~0.92 to 1.48 in the temperature range from 300 to 973 K [205] have been developed at the Jet Propulsion Laboratory (JPL) in Pasadena, California and are being considered for use in Advanced Radio-isotope Power Systems (ARPSs) to support NASA's planetary exploration missions [209]. The use of skutterudite unicouples in the bottom array with SiGe unicouples in the top array has been proposed for cascaded thermoelectric modules (CTMs) for use in radioisotope power systems (RPSs) to generate electric power of 108 W$_e$ and to achieve a net decrease of ~43% in the required amount of ^{238}PuO$_2$ [210]. However, an operational issue with skutterudite-based unicouples is the sublimation of antimony from the legs near the hot junction at ~973 K. Such sublimation could change the thermoelectric properties of the material and degrade the unicouples' performance over time [209]. The use of TEGs in commercial aerospace vehicles, which is expected to reduce fuel consumption by 0.5%, is also being explored by Boeing Research & Technology [211]. As a rough estimate, this fuel savings, if implemented solely in the US, would save passenger and cargo airlines more than $12 million every month and reduce global carbon emissions by 0.03% [212].

7. Conclusion

The use of thermoelectric materials for waste-heat recovery, refrigeration and other applications can aid considerably in global efforts toward energy conservation and the reduction of pollutants. The parameters that affect the performance of thermoelectric materials permit an optimistic outlook for the possibility of obtaining high *ZT* values in materials that are not traditionally qualified as nanomaterials. We have reviewed that principle parameters that have, in the past, driven improvements in the efficiency of TE materials. We have also discussed strategies for improving the Seebeck coefficient, structures that can be used in alloys to decrease their thermal conductivity without modifying their electrical conductivity, and modulation doping to enhance carrier mobility. In addition, we have reviewed the parameters that affect the life expectancy of TE devices, based on the bold assumptions that the shear stress is proportional to the temperature gradient and that the larger the heterogeneity in the thermal expansion coefficient of a material is, the larger is the resultant shear stress. Finally, we have provided an overview of the applications of thermoelectric (TE) modules and their architecture.

References

[1] Xi H, Luo L, Fraisse G. Development and applications of solar-based thermo-electric technologies. Renew Sustain Energy Rev 2007;11:923–36.
[2] Omer AM. Focus on low carbon technologies: the positive solution. Renew Sustain Energy Rev 2008;12:2331–57.
[3] Thirugnanasambandam M, Iniyan S, Goic R. A review of solar thermal technologies. Renew Sustain Energy Rev 2010;14:312–22.
[4] Afshar O, Saidur R, Hasanuzzaman M, Jameel M. A review of thermodynamics and heat transfer in solar refrigeration system. Renew Sustain Energy Rev 2012;16:5639–48.
[5] Kalkan N, Young EA, Celiktas A. Solar thermal air conditioning technology reducing the footprint of solar thermal air conditioning. Renew Sustain Energy Rev 2012;16:6352–83.
[6] Fthenakis V, Kim HC. Life-cycle uses of water in U.S. electricity generation. Renew Sustain Energy Rev 2010;14:2039–48.
[7] Liu D, Zhao F-Y, Tang G-F. Active low-grade energy recovery potential for building energy conservation. Renew Sustain Energy Rev 2010;14:2736–47.
[8] Wang T, Zhang Y, Peng Z, Shu G. A review of researches on thermal exhaust heat recovery with Rankine cycle. Renew Sustain Energy Rev 2011;15:2862–71.
[9] Saidur R, Rezaei M, Muzammil WK, Hassan MH, Paria S, Hasanuzzaman M. Technologies to recover exhaust heat from internal combustion engines. Renew Sustain Energy Rev 2012;16:5649–59.
[10] Vélez F, Segovia JJ, Martín MC, Antolín G, Chejne F, Quijano A. A technical, economical and market review of organic Rankine cycles for the conversion

of low-grade heat for power generation. Renew Sustain Energy Rev 2012;16:4175–89.

[11] Martín-González M, Caballero-Calero O, Díaz-Chao P. Nanoengineering thermoelectrics for 21st century: energy harvesting and other trends in the field. Renew Sustain Energy Rev 2013;24:288–305.

[12] Shu G, Liang Y, Wei H, Tian H, Zhao J, Liu L. A review of waste heat recovery on two-stroke IC engine aboard ships. Renew Sustain Energy Rev 2013;19:385–401.

[13] Riffat SB, Ma X. Thermoelectrics: a review of present and potential applications. Appl Therm Eng 2003;23:913–35.

[14] Dai D, Zhou Y, Liu J. Liquid metal based thermoelectric generation system for waste heat recovery. Renew Energy 2011;36:3530–6.

[15] Tie SF, Tan CW. A review of energy sources and energy management system in electric vehicles. Renew Sustain Energy Rev 2013;20:82–102.

[16] Ullah KR, Saidur R, Ping HW, Akikur RK, Shuvo NH. A review of solar thermal refrigeration and cooling methods. Renew Sustain Energy Rev 2013;24:499–513.

[17] Tsubota T, Ohno T, Shiraishi N, Miyazaki Y. Thermoelectric properties of $Sn_{1-x-y}Ti_ySb_xO_2$ ceramics. J Alloys Compd 2008;463:288–93.

[18] Pichanusakorn P, Bandaru P. Nanostructured thermoelectrics. Mater Sci Eng R: Rep 2010;67:19–63.

[19] Gao X, Uehara K, Klug DD, Tse JS. Rational design of high-efficiency thermoelectric materials with low band gap conductive polymers. Comput Mater Sci 2006;36:49–53.

[20] Zhan G-D, Kuntz JD, Mukherjee AK, Zhu P, Koumoto K. Thermoelectric properties of carbon nanotube/ceramic nanocomposites. Scr Mater 2006;54:77–82.

[21] Snyder GJ, Toberer ES. Complex thermoelectric materials. Nat Mater 2008;7:105–14.

[22] Cai KF, Mueller E, Drasar C, Stiewe C. The effect of titanium diboride addition on the thermoelectric properties of β-FeSi$_2$ semiconductors. Solid State Commun 2004;131:325–9.

[23] Zide D, Vashaee D, Bian Z, Zeng G, Bowers J, Shakouri A, et al. Demonstration of electron filtering to increase the Seebeck coefficient in $In_{0.53}Ga_{0.47}As/In_{0.53}Ga_{0.28}Al_{0.19}As$ superlattices. Phys Rev B 2006;74.

[24] Bian Z, Shakouri A. Enhanced solid-state thermionic emission in nonplanar heterostructures. Appl Phys Lett 2006;88:012102.

[25] Zheng J-C. Recent advances on thermoelectric materials. Front Phys China 2008;3:269–79.

[26] Hochbaum AI, Chen R, Delgado RD, Liang W, Garnett EC, Najarian M, et al. Enhanced thermoelectric performance of rough silicon nanowires. Nature 2008;451:163–7.

[27] Venkatasubramanian R, Siivola E, Colpitts T, O'Quinn B. Thin-film thermoelectric devices with high room-temperature figures of merit. Nature 2001;413:597–602.

[28] Harman TC, Taylor PJ, Walsh MP, LaForge BE. Quantum dot superlattice thermoelectric materials and devices. Science 2002;297:2229–32.

[29] Sootsman JR, Chung DY, Kanatzidis MG. New and old concepts in thermoelectric materials. Angew Chem Int Ed 2009;48:8616–39.

[30] Nolas GS, Morelli DT, Tritt TM. KUTTERUDITES: a phonon-glass-electron crystal approach to advanced thermoelectric energy conversion applications. Annu Rev Mater Sci 1999;29:89–116.

[31] HERWAARDEN VAN, SARRO AW, THERMAL PM. Sensors based on the seebeck effect. Sensors Actuat A: Phys 1986;10:321–46.

[32] Tritt TM, Subramanian MA. Thermoelectric materials, phenomena, and applications: a bird's eye view. MRS Bull 2006;31:188–229.

[33] Pereira Gonçalves A, Branco Lopes E, Rouleau O, Godart C. Conducting glasses as new potential thermoelectric materials: the Cu–Ge–Te case. J Mater Chem 2010;20:1516.

[34] Dmitriev AV, Zvyagin IP. Current trends in the physics of thermoelectric materials. Physics – Uspekhi 2010;53:789–803.

[35] Wan C, Wang Y, Wang N, Koumoto K. Low-thermal-conductivity $(MS)_{1+x}(TiS2)_2$ (M=Pb, Bi, Sn) misfit layer compounds for bulk thermoelectric materials. Materials 2010;3:2606–17.

[36] Bulusu A, Walker DG. Review of electronic transport models for thermoelectric materials. Superlattices Microstruct. 2008;44:1–36.

[37] Ma Y, Hao Q, Poudel B, Lan Y, Yu B, Wang D, et al. Enhanced thermoelectric figure-of-merit in p-type nanostructured bismuth antimony tellurium alloys made from elemental chunks. Nano Lett. 2008;8:2580–4.

[38] Gonçalves AP, Lopes EB, Delaizir G, Vaney JB, Lenoir B, Piarristeguy A, et al. Semiconducting glasses: a new class of thermoelectric materials? J. Solid State Chem. 2012;193:26–30.

[39] Joshi G, Lee H, Lan Y, Wang X, Zhu G, Wang D, et al. Enhanced thermoelectric figure-of-merit in nanostructured p-type silicon germanium bulk alloys. Nano Lett. 2008;8:4670.

[40] Cadoff IB, Miller E. Thermolecteric materials and devices. New York: Reinhold Publishing Corporation; 1960.

[41] Das VD, Ganesan PG. Thickness and temperature effects on thermoelectric power and electrical resistivity of $(Bi_{0.25}Sb_{0.75})_2Te_3$ thin films. Mater Chem Phys 1998;57:57–66.

[42] Kowalczyk A, Falkowski M, Toliński T, Tran VH, Miiller W, Reiffers M, et al. Specific heat, electrical resistivity and thermoelectric power of $YbNi_4Si$. Mater Res Bull 2008;43:185–90.

[43] Wang YF, Lee KH, Ohta H, Koumoto K. Fabrication and thermoelectric properties of heavily rare-earth metal-doped $SrO(SrTiO_3)_n$ ($n=1, 2$) ceramics. Ceram Int 2008;34:849–52.

[44] Watanabe N, Nakayama H, Fukao F, Munakata F. Effects of metal substitution on the electric and thermoelectric properties in $(Ni_{1-x}M_x)Mn_2O_4$ (M=Zn and Mg). Thermochim Acta 2012;532:56–9.

[45] Iversen BB, Palmqvist AEC, Cox DE, Nolas GS, Stucky GD, Blake NP, et al. Why are clathrates good candidates for thermoelectric materials? J Solid State Chem 2000;149:455–8.

[46] Kleinke H. New bulk materials for thermoelectric power generation: clathrates and complex antimonides†. Chem Mater 2010;22:604–11.

[47] Christensen M, Juranyi F, Iversen BB. The rattler effect in thermoelectric clathrates studied by inelastic neutron scattering. Physica B: Condensed Matter 2006;385-386:505–7.

[48] Anno H, Yamada H, Nakabayashi T, Hokazono M, Shirataki R. Gallium composition dependence of crystallographic and thermoelectric properties in polycrystalline type-I $Ba_8Ga_xSi_{46-x}$ (nominal $x=14$–18) clathrates prepared by combining arc melting and spark plasma sintering methods. J Solid State Chem 2012;193:94–104.

[49] Kim SW, Kimura Y, Mishima Y. Effects of doping on the high-temperature thermoelectric properties of $IrSb_3$ skutterudite compounds. J Electron Mater 2003;32:1141–7.

[50] Vaqueiro P, Sobany GG, Powell AV, Knight KS. Structure and thermoelectric properties of the ordered skutterudite $CoGe_{1.5}Te_{1.5}$. J Solid State Chem 2006;179:2047–53.

[51] Kim IH, Park KH, Ur SC. Thermoelectric properties of Sn-doped CoSb3 prepared by encapsulated induction melting. J Alloys Compd 2007;442:351–4.

[52] Ur S-C, Kwon J-C, Kim I-H. Thermoelectric properties of Fe-doped $CoSb_3$ prepared by mechanical alloying and vacuum hot pressing. J Alloys Compd 2007;442:358–61.

[53] Alboni PN, Ji X, He J, Gothard N, Hubbard J, Tritt TM. Synthesis and thermoelectric properties of nano-engineered $CoSb_3$ skutterudite materials. J Electron Mater 2007;36:711–5.

[54] Matsuoka E, Morimoto S, Tanaka K, Sasakawa T, Takabatake T. Magnetic and thermoelectric properties of $Ba_yFe_{4-x}Co_xSb_{12}$. Physica B: Condensed Matter 2006;383:132–3.

[55] Park K-H, Kim I-H. Thermoelectric properties of Ca-filled $CoSb_3$-based skutterudites synthesized by mechanical alloying. J Electron Mater 2010;40:493–8.

[56] Kim SW, Kimura Y, Mishima Y. Effect of partial La filling on high-temperature thermoelectric properties of $IrSb_3$-based skutterudite compounds. J Electron Mater 2004;33:1156–60.

[57] Alleno E, Bérardan D, Godart C, Puyet M, Lenoir B, Lackner R, et al. Double filling in skutterudites: a promising path to improved thermoelectric properties. Physica B: Condensed Matter 2006;383:103–6.

[58] Sklad AC, Gaultois MW, Grosvenor AP. Examination of CeFe4Sb12 upon exposure to air: is this material appropriate for use in terrestrial, high-temperature thermoelectric devices? J Alloys Compd, 505; 2010; L6–9.

[59] Rogl G, Grytsiv A, Rogl P, Bauer E, Zehtbauer M. A new generation of p-type didymium skutterudites with high *ZT*. Intermetallics 2011;19:546–55.

[60] Grytsiv A, Rogl P, Berger S, Paul C, Michor H, Bauer E, et al. Novel thermoelectric skutterudites $Sn_yNi_4Sb_{12-x}Sn_x$. Physica B: Condensed Matter 2003;328:71–3.

[61] Jung J-Y, Ur S-C, Kim I-H. Thermoelectric properties of InzCo4Sb12−yTey skutterudites. Mater Chem Phys 2008;108:431–4.

[62] Lu P-X, Wu F, Han H-L, Wang Q, Shen Z-G, Hu X. Thermoelectric properties of rare earths filled $CoSb_3$ based nanostructure skutterudite. J Alloys Compd 2010;505:255–8.

[63] Liu K, Dong X, Jiuxing Z. The effects of La on thermoelectric properties of LaxCo4Sb12 prepared by MA–SPS. Mater Chem Phys 2006;96:371–5.

[64] Ravot D, Lafont U, Chapon L, Tedenac JC, Mauger A. Anomalous physical properties of cerium–lanthanum filled skutterudites. J Alloys Compd 2001;323–324:389–91.

[65] Bai SQ, Pei YZ, Chen LD, Zhang WQ, Zhao XY, Yang J. Enhanced thermoelectric performance of dual-element-filled skutterudites BaxCeyCo4Sb12. Acta Mater 2009;57:3135–9.

[66] Ballikaya S, Uzar N, Yildirim S, Salvador JR, Uher C. High thermoelectric performance of In, Yb, Ce multiple filled CoSb3 based skutterudite compounds. J Solid State Chem 2012;193:31–5.

[67] Chakoumakos BC, Sales BC. Skutterudites: their structural response to filling. J Alloys Compd 2006;407:87–93.

[68] Deng L, Jia XP, Su TC, Jiang YP, Zheng SZ, Guo X, et al. The thermoelectric properties of $Co_4Sb_{12-x}Te_x$ synthesized at different pressure. Mater Lett 2011;65:1057–9.

[69] Wojciechowski KT, Toboła J, Leszczyński J. Thermoelectric properties and electronic structure of CoSb3 doped with Se and Te. J Alloys Compd 2003;361:19–27.

[70] Kitagawa H, Wakatsuki M, Nagaoka H, Noguchi H, Isoda Y, Hasezaki K, et al. Temperature dependence of thermoelectric properties of Ni-doped $CoSb_3$. J Phys Chem Solids 2005;66:1635–9.

[71] Peng J, Yang J, Zhang T, Song X, Chen Y. Preparation and characterization of Fe substituted CoSb3 skutterudite by mechanical alloying and annealing. J Alloys Compd 2004;381:313–6.

[72] Yu J, Zhao W, Zhou H, Wei P, Zhang Q. Rapid preparation and thermoelectric properties of Ba and In double-filled p-type skutterudite bulk materials. Scr Mater 2013;68:643–6.

[73] Shi X, Salvador JR, Yang J, Wang H. Thermoelectric properties of n-type multiple-filled Skutterudites. J Electron Mater 2009;38:930–3.

[74] Shi X, Yang J, Salvador JR, Chi M, Cho JY, Wang H, et al. Multiple-filled skutterudites: high thermoelectric figure of merit through separately optimizing electrical and thermal transports. J Am Chem Soc 2011;133:7837–46.

[75] Zou M, Li J-F, Kita T. Thermoelectric properties of fine-grained FeVSb half-Heusler alloys tuned to p-type by substituting vanadium with titanium. J Solid State Chem 2013;198:125–30.

[76] Wang S-H, Cheng H-M, Wu R-J, Chao W-H. Structural and thermoelectric properties of HfNiSn half-Heusler thin films. Thin Solid Films 2010;518: 5901–4.

[77] Kawaharada Y, Kurosaki K, Muta H, Uno M, Yamanaka S. High temperature thermoelectric properties of $CoNb_{1-x}Hf_xSn_{1-y}Sb_y$ half-Heusler compounds. J Alloys Compd 2004;377:312–5.

[78] Shutoh N, Sakurada S. Thermoelectric properties of the $TiX(Zr_{0.5}Hf_{0.5})_{1-x}NiSn$ half-Heusler compounds. J Alloys Compd 2005;389:204–8.

[79] Lee P-J, Chao L-S. High-temperature thermoelectric properties of Ti0.5(ZrHf) 0.5 − xNbxNi0.9Pd0.1Sn0.98Sb0.02 half-Heusler alloys. J Alloys Compd 2010;504:192–6.

[80] Fu C, Xie H, Liu Y, Zhu TJ, Xie J, Zhao XB. Thermoelectric properties of FeVSb half-Heusler compounds by levitation melting and spark plasma sintering. Intermetallics 2013;32:39–43.

[81] Maji P, Takas NJ, Misra DK, Gabrisch H, Stokes K, Poudeu PFP. Effects of Rh on the thermoelectric performance of the p-type $Zr_{0.5}Hf_{0.5}Co_{1-x}Rh_xSb_{0.99}Sn_{0.01}$ half-Heusler alloys. J Solid State Chem 2010;183:1120–6.

[82] Nylén J, Lidin S, Andersson M, Liu H, Newman N, Häussermann U. Effect of metal doping on the low-temperature structural behavior of thermoelectric β-Zn_4Sb_3. J Solid State Chem 2007;180:2603–15.

[83] Carreon H. On the exploitation of thermoelectric coupling for characterization of elliptical inclusions in metals. Expl Therm Fluid Sci 2013;44:673–9.

[84] Ferreira NM, Rasekh S, Costa FM, Madre MA, Sotelo A, Diez JC, et al. New method to improve the grain alignment and performance of thermoelectric ceramics. Mater Lett 2012;83:144–7.

[85] Liu S, Wang J, Jia J, Hu X, Liu S. Synthesis and thermoelectric performance of Li-doped NiO ceramics. Ceram Int 2012;38:5023–6.

[86] Wang HC, Wang CL, Su WB, Liu J, Zhao Y, Peng H, et al. Enhancement of thermoelectric figure of merit by doping Dy in La0.1Sr0.9TiO3 ceramic. Mater Res Bull 2010;45:809–12.

[87] Constantinescu G, Rasekh S, Torres MA, Madre MA, Diez JC, Sotelo A. Enhancement of the high-temperature thermoelectric performance of $Bi_2Ba_2Co_2O_x$ ceramics. Scr Mater 2013;68:75–8.

[88] Kenfaui D, Chateigner D, Gomina M, Noudem JG. Texture mechanical and thermoelectric properties of $Ca_3Co_4O_9$ ceramics. J Alloys Compd 2010;490: 472–9.

[89] Li F, Li J-F. Effect of Ni substitution on electrical and thermoelectric properties of $LaCoO_3$ ceramics. Ceram Int 2011;37:105–10.

[90] Liu J, Wang CL, Su WB, Wang HC, Li JC, Zhang JL, et al. Thermoelectric properties of $Sr_{1-x}Nd_xTiO_3$ ceramics. J Alloys Compd 2010;492:L54–6.

[91] Tajima S, Tani T, Isobe S, Koumoto K. Thermoelectric properties of highly textured $NaCo_2O_4$ ceramics processed by the reactive templated grain growth (RTGG) method. Mater Sci Eng 2001;B86:20–5.

[92] Wang LM, Chang C-Y, Yeh S-T, Chen SW, Peng ZA, Bair SC, et al. Synthesis and post-annealing effects on the transport properties of thermoelectric oxide $(ZnO)mIn_2O_3$ ceramics. Ceram Int 2012;38:1167–74.

[93] Yasukawa M, Kono T. Preparation of dense $BaPbO_3$-based ceramics by a coprecipitation and their thermoelectric properties. J Alloys Compd 2006;426:420–5.

[94] Yasukawa M, Kono T, Ueda K, Yanagi H, Hosono H. High-temperature thermoelectric properties of La-doped $BaSnO_3$ ceramics. Mater Sci Eng B 2010;173:29–32.

[95] Wang N, He H, Li X, Han L, Zhang C. Enhanced thermoelectric properties of Nb-doped $SrTiO_3$ polycrystalline ceramic by titanate nanotube addition. J Alloys Compd 2010;506:293–6.

[96] Delorme F, Martin CF, Marudhachalam P, Ovono DO, Guzman G. Effect of Ca substitution by Sr on the thermoelectric properties of $Ca_3Co_4O_9$ Ceramics. J Alloys Compd 2011;509:2311–5.

[97] Noudem JG, Lemonnier S, Prevel M, Reddy ES, Guilmeau E, Goupil C. Thermoelectric ceramics for generators. J Eur Ceram Soc 2008;28:41–8.

[98] Tsai T-C, Chang H-C, Chen C-H, Whang W-T. Widely variable Seebeck coefficient and enhanced thermoelectric power of PEDOT:PSS films by blending thermal decomposable ammonium formate. Org Electron 2011;12:2159–64.

[99] Choi Y, Kim Y, Park S-G, Kim Y-G, Sung BJ, Jang S-Y, et al. Effect of the carbon nanotube type on the thermoelectric properties of CNT/Nafion nanocomposites. Org Electron 2011;12:2120–5.

[100] Yue R, Xu J. Poly(3,4-ethylenedioxythiophene) as promising organic thermoelectric materials: a mini-review. Synth Met 2012;162:912–7.

[101] Chatterjee K, Suresh A, Ganguly S, Kargupta K, Banerjee D. Synthesis and characterization of an electro-deposited polyaniline-bismuth telluride nanocomposite — a novel thermoelectric material. Mater Charact 2009;60: 1597–601.

[102] Du Y, Shen SZ, Cai K, Casey PS. Research progress on polymer–inorganic thermoelectric nanocomposite materials. Prog Polym Sci 2012;37:820–41.

[103] Zhang KX, Qin XY, Xin HX, Li HJ, Zhang J. Transport and thermoelectric properties of nanocrystal substitutional semiconductor alloys $(Mg_{1-x}Cd_x)_3Sb_2$ doped with Ag. J Alloys Compd 2009;484:498–504.

[104] Chen L, Li J, Sun F, Wu C. Performance optimization of a two-stage semiconductor thermoelectric-generator. Appl Energy 2005;82:300–12.

[105] Dughaish ZH. Lead telluride as a thermoelectric material for thermoelectric power generation. Physica B 2005;322:205–23.

[106] Majumdar A. Thermoelectricity in semiconductor nanostructures. Mater Sci 2004;303:777–8.

[107] Alam H, Ramakrishna S. A review on the enhancement of figure of merit from bulk to nano-thermoelectric materials. Nano Energy 2013;2:190–212.

[108] Tani J-i Kido H. Thermoelectric properties of Bi-doped Mg_2Si semiconductors. Physica B: Condensed Matter 2005;364:218–24.

[109] Ozpineci B, Tolbert LM. Comparison of wide-bandgap semiconductors for power electronics applications. Oak Ridge National Laboratory; 2003.

[110] Omar MS, Gorges FY. The optical energy gap dependence on both carrier concentration and intrinsic energy gap in n-type semiconductors. Mater Sci Semiconduct Process 2006;9:164–7.

[111] Gao Y, Ying P, Cui J, Chen S, Li Y. Thermoelectric properties of Cu and Sb Co-doped Ga-Te based semiconductor with wide band gap. Proc Eng 2012;27: 156–62.

[112] Hummel RE. Electronic properties of materials. 3rd edition. New York: Springer; 2011.

[113] Nag BR. Direct band-gap energy of semiconductors. Infrared Phys Technol 1995;36:831–5.

[114] Zhang FP, Lu QM, Zhang X, Zhang JX. First principle investigation of electronic structure of CaMnO3 thermoelectric compound oxide. J Alloys Compd 2011;509:542–5.

[115] Ramdas AK, Rodriguez S, Tsoi S, Haller EE. Electronic band gaps of semiconductors as influenced by their isotopic composition. Solid State Commun 2005;133:709–14.

[116] Tan G, Wang S, Yan Y, Li H, Tang X. Enhanced thermoelectric performance in p-type $Ca_{0.5}Ce_{0.5}Fe_{4-x}Ni_xSb_{12}$ skutterudites by adjusting the carrier concentration. J Alloys Compd 2012;513:328–33.

[117] Wang S, Fu F, She X, Zheng G, Li H, Tang X. Optimizing thermoelectric performance of Cd-doped β-Zn4Sb3 through self-adjusting carrier concentration. Intermetallics 2011;19:1823–30.

[118] Delaizir G, Bernard-Granger G, Monnier J, Grodzki R, Kim-Hak O, Szkutnik PD, et al. A comparative study of Spark Plasma Sintering (SPS), Hot Isostatic Pressing (HIP) and microwaves sintering techniques on p-type Bi2Te3 thermoelectric properties. Mater Res Bull 2012;47:1954–60.

[119] Drasar C, Kucek V, Benes L, Lostak P, Vlcek Mb. Thermoelectric properties and nonstoichiometry of GaGeTe. J Solid State Chem 2012;193:42–6.

[120] Roudebush JH, Toberer ES, Hope H, Jeffrey Snyder G, Kauzlarich SM. Crystal structure, characterization and thermoelectric properties of the type-I clathrate $Ba_{8-y}Sr_yAl_{14}Si_{32}$ $(0.6 \le y \le 1.3)$ prepared by aluminum flux. J Solid State Chem 2011;184:1176–85.

[121] Mikhnovich Jr. VV. Scattering of charge carriers in semiconductors: models and their criteria. Physica 2001;B 308–310:1023–6.

[122] Karl N. Charge carrier transport in organic semiconductors. Synth Met 2003;133–134:649–57.

[123] Uberuaga BP, Henkelman G, Jo´nsson H, Dunham ST, Windl W, Stumpf R. Theoretical studies of self-diffusion and dopant clustering in semiconductors. Phys stat sol 2002;233:24–30.

[124] Bracht HA, Silvestri HH, Haller EE. Advanced diffusion studies with isotopically controlled materials. Solid State Commun 2005;133:727–35.

[125] Cui JL, Zhao XB, Zhao WM, Lu YP. Preparation, thermoelectric properties and interface analysis of n-type graded material FeSi2/Bi2Te3. Mater Sci Eng 2002; B94:223–8.

[126] Nakagawa T, Sakaguchi I, Matsunaga K, Yamamoto T, Haneda H, Ikuhara Y. Control of point defects and grain boundaries in advanced materials. Nucl Inst Meth Phys Res Sect B: Beam Inter Mater Atoms 2005;232:343–7.

[127] Wanwan L, Zechun C, Bin Z, Feng Z, Hongtao L, Wenbin S, et al. Study on the effect of Cd-diffusion annealing on the electrical properties of CdZnTe. J Crystal Growth 2006;292:53–61.

[128] Bae N-H, Han S, Lee KE, Kim B, Kim S-T. Diffusion at interfaces of micro thermoelectric devices. Curr Appl Phys 2011;11:S40–4.

[129] Xu Z, Lan Z, Zhu G, Sun K, Yu Z. Effects of the oxygen partial pressure during deposition on the material characteristics and magnetic properties of BaM thin films. J Alloys Compd 2012;538:11–5.

[130] Terasaki I. Transport properties and electronic states of the thermoelectric oxide NaCo2O4. Physica B: Condensed Matter 2003;328:63–7.

[131] Ito M, Furumoto D. Effects of noble metal addition on microstructure and thermoelectric properties of NaxCo2O4. J Alloys Compd 2008;450:494–8.

[132] Zhou XF, Zhang H, Chen QM, Shang J, Zhang PX. Effects of annealing atmosphere on thermoelectric signals from ZnO films. Thin Solid Films 2011;519:3026–8.

[133] Li FM, Waddingham R, Milne WI, Flewitt AJ, Speakman S, Dutson J, et al. Low temperature (< 100 °C) deposited P-type cuprous oxide thin films: importance of controlled oxygen and deposition energy. Thin Solid Films 2011;520:1278–84.

[134] Liu HJ, Song CM, Wu ST, Li LF. Processing method dependency of thermoelectric properties of Bi85Sb15 alloys in low temperature. Cryogenics 2007;47:56–60.

[135] Prokhorov VM, Pivovarov GI. Detection of internal cracks and ultrasound characterization of nanostructured Bi2Te3-based thermoelectrics via acoustic microscopy. Ultrasonics 2011;51:715–8.

[136] Moon C, Shin S, Kim D, Kim T-S. Microstructure and thermoelectric properties of p-type Bi2Te3–Sb2Te3 alloys produced by rapid solidification and spark plasma sintering. J Alloys Compd 2010;504:S504–7.

[137] Kim T-S, Chun B-S. Microstructure and thermoelectric properties of n- and p-type Bi$_2$Te$_3$ alloys by rapid solidification processes. J Alloys Compd 2007;437:225–30.

[138] Ren F, Case ED, Timm EJ, Schock HJ. Hardness as a function of composition for n-type LAST thermoelectric material. J Alloys Compd 2008;455:340–5.

[139] Zhou D, Liu J, Xu S, Peng P. Thermal stability and elastic properties of Mg$_2$X (X=Si, Ge, Sn, Pb) phases from first-principle calculations. Comput Mater Sci 2012;51:409–14.

[140] Fan X, Case ED, Ren F, Shu Y, Baumann MJ, Part II. Fracture strength and elastic modulus as a function of porosity for hydroxyapatite and other brittle materials. J Mech Behav Biomed Mater 2012;8:99–110.

[141] Hong S-J, Lee S-H, Chun B-S. Thermoelectric properties of newly fabricated n-type 95%Bi$_2$Te$_2$–5%Bi$_2$Se$_3$ alloys by gas atomizing and extrusion process. Mater Sci Eng B 2003;98:232–8.

[142] Zhao D, Li X, He L, Jiang W, Chen L. Interfacial evolution behavior and reliability evaluation of CoSb$_3$/Ti/Mo–Cu thermoelectric joints during accelerated thermal aging. J Alloys Compd 2009;477:425–31.

[143] Zhao D, Geng H, Teng X. Fabrication and reliability evaluation of CoSb$_3$/W–Cu thermoelectric element. J Alloys Compd 2012;517:198–203.

[144] Zhu T, Li J. Ultra-strength materials. Prog Mater Sci 2010;55:710–57.

[145] Jung D-y Kurosaki K, Kim C-e, Muta H, Yamanaka S. Thermal expansion and melting temperature of the half-Heusler compounds: MNiSn (M=Ti, Zr, Hf). J Alloys Compd 2010;489:328–31.

[146] Huang M-J, Chou P-K, Lin M-C. Thermal and thermal stress analysis of a thin-film thermoelectric cooler under the influence of the Thomson effect. Sens Actuat A: Phys 2006;126:122–8.

[147] Al-Merbati AS, Yilbas BS, Sahin AZ. Thermodynamics and thermal stress analysis of thermoelectric power generator: influence of pin geometry on device performance. Appl Therm Eng 2013;50:683–92.

[148] Asenath-Smith E, Misture ST, Edwards DD. Structural behavior and thermo-electric properties of the brownmillerite system Ca$_2$(Zn$_x$Fe$_{2-x}$)O$_5$. J Solid State Chem 2011;184:2167–77.

[149] Tachibana M, Fang J. An estimation of thermal stress of thermoelectric devices in the temperature cycling test. Proc Eng 2012;27:177–85.

[150] Rogl G, Aabdin Z, Schafler E, Horky J, Setman D, Zehetbauer M, et al. Effect of HPT processing on the structure, thermoelectric and mechanical properties of Sr$_{0.07}$Ba$_{0.07}$Yb$_{0.07}$Co$_4$Sb$_{12}$. J Alloys Compd 2012;537:183–9.

[151] Ahiska R, Dislitas S, Omer G. A new method and computer-controlled system for measuring the time constant of real thermoelectric modules. Energy Convers Manage 2012;53:314–21.

[152] Chein R, Huang G. Thermoelectric cooler application in electronic cooling. Appl Therm Eng 2004;24:2207–17.

[153] Putra N, Yanuar, Iskandar FN. Application of nanofluids to a heat pipe liquid-block and the thermoelectric cooling of electronic equipment. Exp Therm Fluid Sci 2011;35:1274–81.

[154] Zhang HY, Mui YC, Tarin M. Analysis of thermoelectric cooler performance for high power electronic packages. Appl Therm Eng 2010;30:561–8.

[155] PrezAparicio JL, Palma R, Taylor RL. Finite element analysis and material sensitivity of Peltier thermoelectric cells coolers. Int J Heat Mass Transf 2012;55:1363–74.

[156] Chang Y-W, Chang C-C, Ke M-T, Chen S-L. Thermoelectric air-cooling module for electronic devices. Appl Therm Eng 2009;29:2731–7.

[157] Huang H-S, Weng Y-C, Chang Y-W, Chen S-L, Ke M-T. Thermoelectric water-cooling device applied to electronic equipment. Int Commun Heat Mass Transf 2010;37:140–6.

[158] Zhou Y, Yu J. Design optimization of thermoelectric cooling systems for applications in electronic devices. Int J Refrig 2012;35:1139–44.

[159] Wang X, Yu J, Ma M. Optimization of heat sink configuration for thermo-electric cooling system based on entropy generation analysis. Int J Heat Mass Transf 2013;63:361–5.

[160] Abdul-Wahab SA, Elkamel A, Al-Damkhi AM, IhA Al-Habsi, Al-Rubai'ey HS, Al-Battashi AK, et al. Design and experimental investigation of portable solar thermoelectric refrigerator. Renew Energy 2009;34:30–4.

[161] Dai YJ, Wang RZ, Ni L. Experimental investigation on a thermoelectric refrigerator driven by solar cells. Renew Energy 2003;28:949–59.

[162] Chen L, Meng F, Sun F. Effect of heat transfer on the performance of thermoelectric generator-driven thermoelectric refrigerator system. Cryogenics 2012;52:58–65.

[163] Luo T, Wang S, Li H, Tang X. Low temperature thermoelectric properties of melt spun Bi85Sb15 alloys. Intermetallics 2013;32:96–102.

[164] Meng F, Chen L, Sun F. Performance prediction and irreversibility analysis of a thermoelectric refrigerator with finned heat exchanger. Acta Phys Pol A 2011;120:397–406.

[165] Available at www.tetech.com; 2010.

[166] Shen L, Xiao F, Chen H, Wang S. Investigation of a novel thermoelectric radiant air-conditioning system. Energy Build 2013;59:123–32.

[167] Riffat SB, Qiu G. Comparative investigation of thermoelectric air-conditioners versus vapour compression and absorption air-conditioners. Appl Therm Eng 2004;24:1979–93.

[168] Cherkez R. Theoretical studies on the efficiency of air conditioner based on permeable thermoelectric converter. Appl Therm Eng 2012;38:7–13.

[169] Niu X, Yu J, Wang S. Experimental study on low-temperature waste heat thermoelectric generator. J Power Sources 2009;188:621–6.

[170] Vullers RJM, van Schaijk R, Doms I, Van Hoof C, Mertens R. Micropower energy harvesting. Solid-State Electron 2009;53:684–93.

[171] Snyder GJ. Small thermoelectric generators. Interface: the electrochemical society, Fall; 2008. p. 54–6.

[172] Group A-hW. Critical raw materials for the EU. European Commission; 2010.

[173] Yu C, Chau KT. Thermoelectric automotive waste heat energy recovery using maximum power point tracking. Energy Convers Manage 2009;50:1506–12.

[174] Hsu C-T, Huang G-Y, Chu H-S, Yu B, Yao D-J. Experiments and simulations on low-temperature waste heat harvesting system by thermoelectric power generators. Appl Energy 2011;88:1291–7.

[175] Karri MA, Thacher EF, Helenbrook BT. Exhaust energy conversion by thermo-electric generator: two case studies. Energy Convers Manage 2011;52:1596–611.

[176] Gou X, Yang S, Xiao H, Ou Q. A dynamic model for thermoelectric generator applied in waste heat recovery. Energy 2013;52:201–9.

[177] Yee SK, LeBlanc S, Goodson KE, Dames C. $ per W metrics for thermoelectric power generation: beyond ZT. Energy Environ Sci 2013;6:2561.

[178] Sano S, Mizukami H, Kaibe H. Development of high-efficiency thermoelectric power generation system. KOMAT'SU; 2003.

[179] Omer SA, Infield DG. Design optimization of thermoelectric devices for solar power generation. Solar Energy Mater Solar Cells 1998;53:67–82.

[180] Omer SA, Infield DG. Design and thermal analysis of a two stage solar concentrator for combined heat and thermoelectric power generation. Energy Convers Manage 2000;41:737–56.

[181] Suter C, Tomeš P, Weidenkaff A, Steinfeld A. Heat transfer and geometrical analysis of thermoelectric converters driven by concentrated solar radiation. Materials 2010;3:2735–52.

[182] He W, Su Y, Wang YQ, Riffat SB, Ji J. A study on incorporation of thermo-electric modules with evacuated-tube heat-pipe solar collectors. Renew Energy 2012;37:142–9.

[183] Kraemer D, McEnaney K, Chiesa M, Chen G. Modeling and optimization of solar thermoelectric generators for terrestrial applications. Solar Energy 2012;86:1338–50.

[184] Xiao J, Yang T, Li P, Zhai P, Zhang Q. Thermal design and management for performance optimization of solar thermoelectric generator. Appl Energy 2012;93:33–8.

[185] Deng Y, Zhu W, Wang Y, Shi Y. Enhanced performance of solar-driven photovoltaic–thermoelectric hybrid system in an integrated design. Solar Energy 2013;88:182–91.

[186] Miljkovic N, Wang EN. Modeling and optimization of hybrid solar thermo-electric systems with thermosyphons. Solar Energy 2011;85:2843–55.

[187] Faïd F, Romdhane M, Gourdon C, Wilhelm AM, Delmas H. A comparative study of local sensors of power ultrasound effects electrochemical, thermo-electrical and chemical probes. Ultrason Sonochem 1998;5:63–8.

[188] Ahamat MA, Tierney MJ. Timewise temperature control with heat metering using a thermoelectric module. Appl Thermal Eng 2011;31:1421–6.

[189] Vancauwenberghe O, Short J, Giehler E, Bildstein P, Ancey P, Gschwind M. Microsensor for the preventive detection of water condensation: operating principle and interface electronics. Sens Actuat A 1996;53:304–8.

[190] Sawaguchi N, Shin W, Izu N, Matsubara I, Murayama N. Effect of humidity on the sensing property of thermoelectric hydrogen sensor. Sens Actuat B: Chem 2005;108:461–6.

[191] Stachowiak H, Lassue S, Dubernard A, Gaviot E. A thermoelectric sensor for fluid flow measurement. principles, calibration and solution for self temperature compensation. Flow Meas Instrum 1998;9:135–41.

[192] Jacobs T, Kutzner C, Kropp M, Brokmann G, Lang W, Steinke A, et al. Combination of a novel perforated thermoelectric flow and impedimetric sensor for monitoring chemical conversion in micro fluidic channels. Proc Chem 2009;1:1127–30.

[193] Jacobs T, Kutzner C, Kropp M, Lang W, Kienle A, Hauptmann P. Novel pressure stable thermoelectric flow sensor in non-steady state operation mode for inline process analysis in micro reactors. Proc Chem 2009;1:148–51.

[194] Mülller M, Budde W, Gotffried-Gottfried R, Hübel A, Jähne R, Kück H. A thermoelectric infrared radiation sensor with monolithically integrated amplifier stage and temperature sensor. Sens Actuat A 1996;54:601–5.

[195] Escriba C, Campo E, Estève D, Fourniols JY. Complete analytical modeling and analysis of micromachined thermoelectric uncooled IR sensors. Sens Actuat A: Phys 2005;120:267–76.

[196] Hirota M, Nakajima Y, Saito M, Uchiyama M. 120 × 90 element thermo-electric infrared focal plane array with precisely patterned Au-black absorber. Sens Actuat A: Phys 2007;135:146–51.

[197] Ploteau JP, Glouannec P, Noel H. Conception of thermoelectric flux meters for infrared radiation measurements in industrial furnaces. Appl Therm Eng 2007;27:674–81.

[198] Ihring A, Kessler E, Dillner U, Haenschke F, Schinkel U, Meyer H-G. Surface-micromachined thermoelectric infrared focal-plane array with high detectivity for room temperature operation. Microelectron Eng 2011;88:2267–71.

[199] Sion C, Godts P, Ziouche K, Bougrioua Z, Lasri T, Leclercq D. Unpackaged infrared thermoelectric microsensor realised on suspended membrane by silicon technology. Sens Actuat A: Phys 2012;175:78–86.

[200] Kopparthy VL, Tangutooru SM, Nestorova GG, Guilbeau EJ. Thermoelectric microfluidic sensor for bio-chemical applications. Sens Actuat B: Chem 2012;166-167:608–15.

[201] Kozlov AG. Optimization of thin-film thermoelectric radiation sensor with comb thermoelectric transducer. Sens Actuat 1999;75:139–50.

[202] Kozlov AG. Optimization of thin-film thermoelectric radiation sensor with separate disposition of absorbing layer and comb thermoelectric transducer. Sens Actuat 2000;84:259–69.

[203] El-Genk MS, Saber HH. Performance analysis of cascaded thermoelectric converters for advanced radioisotope power systems. Energy Convers Manage 2005;46:1083–105.

[204] O'Brien RC, Ambrosi RM, Bannister NP, Howe SD, Atkinson HV. Safe radio-isotope thermoelectric generators and heat sources for space applications. J Nucl Mater 2008;377:506–21.

[205] El-Genk MS, Saber HH, Caillat T. Efficient segmented thermoelectric unicouples for space power applications. Energy Convers Manage 2003;44:1755–72.

[206] Rinehart GH. Design characteristics and fabrication of radioisotope heat sources for space missions. Prog Nucl Energy 2001;39:305–19.

[207] Lange RG, Carroll WP. Review of recent advances of radioisotope power systems. Energy Convers Manage 2008;49:393–401.

[208] Bennett GL, Hemler RJ, Schock A. Status report on the U.S. space nuclear program. Acta Astronaut 1996;38:551–60.

[209] El-Genk MS, Saber HH, Caillat T, Sakamoto J. Tests results and performance comparisons of coated and un-coated skutterudite based segmented uni-couples. Energy Convers Manage 2006;47:174–200.

[210] El-Genk MS, Saber HH. Thermal and performance analyses of efficient radioisotope power systems. Energy Convers Manage 2006;47:2290–307.

[211] Huang J. Aerospace and aircraft thermoelectric applications, Thermoelectrics applications Workshop. San Diego, CA: The Boeing Company; 2009.

[212] Kousksou T, Bédécarrats J-P, Champier D, Pignolet P, Brillet C. Numerical study of thermoelectric power generation for an helicopter conical nozzle. J Power Sources 2011;196:4026–32.